International Journal of Non-Linear Mechanics 118 (2020) 103276

Contents lists available at ScienceDirect

International Journal of Non-Linear Mechanics

journal homepage: www.elsevier.com/locate/nlm

Nonlinear dynamics of an inclined FG pipe conveying pulsatile hot fluid

Rajidi Shashidhar Reddy, Satyajit Panda *, Abhay Gupta

Department of Mechanical Engineering, Indian Institute of Technology Guwahati, India

ARTICLE INFO

Keywords:
Functionally graded pipes
Inclined pipes
Fluid conveying pipes
Nonlinear dynamics of pipes

ABSTRACT

In this theoretical work, the nonlinear dynamics of a pinned–pinned inclined functionally graded (FG) pipe conveying pulsatile hot fluid is investigated. The equation of motion of the FG pipe is derived based on the Euler–Bernoulli beam theory and plug-flow model, and that is subsequently solved using Galerkin discretization in conjunction with the incremental harmonic balance/Runge–Kutta method. First, the divergence of the FG pipe is investigated where it is mainly revealed that the inclination of the pipe with the vertical axis yields buckling at a higher temperature while the type of the associated bifurcation changes from pitchfork to saddle–node bifurcation. On the basis of this static instability, the pre- and post-buckled equilibriums of the inclined FG pipe are identified, and its nonlinear dynamics associated with each of these equilibrium states is subsequently studied based on the variations of some system parameters namely inclination angle, temperature, graded exponent of FG material, mean flow velocity, amplitude of pulsatile flow velocity and material damping. The corresponding results reveal some notable nonlinear dynamic characteristics of the inclined FG pipe like the appearance of both the principal primary and secondary parametric resonances in the pre-buckled state, exchange between softening and hardening structural behavior through period doubling/period demultiplying/fold bifurcation, movement of saddle periodic orbit with temperature leading to the unequal domains of attraction over the post-buckled equilibriums and the appearance higher order parametric resonances at low material damping.

1. Introduction

Pipes conveying steady or pulsatile fluid at moderate or high velocities are common elements in petrochemical industries, oil and gas industries, ocean mining, rocket and aircraft engines, power generating systems, etc. These flexible slender cylindrical elements are often susceptible to undergo instability due to the flow induced vibration. As it may lead to the failure of the associated engineering systems, the flow induced vibration of slender pipes has attracted the attention of many researchers leading to a good number of studies on the linear and nonlinear dynamics of fluid conveying pipes [1–6]. From these available studies, it is known that the internal steady flow typically causes static (divergence) or dynamic (flutter) instability of a pipe beyond a certain flow velocity. The former one (divergence) appears for a pipe supported at its both ends [7] while the later one (flutter) arises for a cantilever pipe [8,9]. However, in many practical piping systems, the fluid flows with pulsatile velocity due to the bends, valves, pumps, change of cross-section, etc. This pulsatile fluid flow is usually attributed by a harmonic component of velocity over the mean flow velocity, and it induces dynamic compressive stresses in a pipe leading to the parametric resonance or instability [3,10]. This type of dynamic instability is usually characterized by the parametric instability region that is basically a domain of pulsation amplitude and frequency of pulsatile fluid flow, and the effects of different system parameters on the parametric instability zone are the major concerns in the linear analysis [11,12]. Besides, the nonlinear vibration of the pipes via the parametric resonance has also been studied by many researchers [13–17]. The corresponding nonlinear dynamics of the pipe may appear in a complex manner once the pipe undergoes divergence at some critical flow velocity. A good number of research reports in this direction have been addressed in the literature [18–25].

In some engineering systems like steam generators, heat exchangers, liquid propellant rocket engines, etc., the associated pipe systems operate under the internal and/or external flow of hot fluid. In these applications of pipes, a pipe is subjected to the thermally induced compressive stress as well as the similar stress due to the velocity of fluid flow. However, the effect of the temperature is indicatively more than that of the velocity in causing the divergence (buckling) of the pipe so that it (pipe) may undergo buckling at very low velocity of a hot fluid [26], and also it (pipe) may exhibit complex nonlinear dynamics associated with its divergence even at a very low pulsatile velocity of hot fluid. So, the temperature is the major concern rather than the velocity of the fluid in the design of these pipe systems conveying hot fluid.

* Correspondence to: Department of Mechanical Engineering, I. I. T. Guwahati, Guwahati 781039, India.
E-mail address: spanda@iitg.ac.in (S. Panda).

https://doi.org/10.1016/j.ijnonlinmec.2019.103276
Received 10 May 2019; Received in revised form 13 September 2019; Accepted 13 September 2019
Available online 20 September 2019
0020-7462/© 2019 Elsevier Ltd. All rights reserved.

In order to alleviate this thermally induced static instability and the associated complex motion of a fluid conveying pipe, it (pipe) can be made of the functionally graded material (FGM) [27], where the FGM is made of two isotropic constituent materials namely metal and ceramic so that the hot surface of the pipe is made of ceramic constituent and the material properties vary gradually from ceramic to metal across the wall-thickness of the pipe. This FGM pipe can withstand against a high temperature of the fluid due to the ceramic constituent while its toughness is retained by the metal constituent. So, the stability of the pipe conveying hot fluid would improve and also it (pipe) can sustain the flow induced vibration. However, a very few studies on this issue are available in the literature. Hosseini and Fazelzadeh [28] investigated the thermo-mechanical stability of a cantilever FG pipe conveying steady flow under thermal environment. Later, Eftekhari and Hosseini [29] reported a similar study on the thermo-mechanical stability of a cantilever FG pipe spinning about its longitudinal axis. These studies reveal indicative improvement of thermo-mechanical stability of the pipe when it is made of FGM instead of conventional isotropic material. Apart from these studies, further investigation on the dynamics of FG pipes conveying steady or pulsatile hot fluid is not available in the literature to the best knowledge of authors.

A straight pipe is usually laid either of the horizontal, vertical and inclined orientations as that appear in many industrial piping systems [30–35]. However, the dynamic behavior of an inclined pipe is somewhat different from that of the vertical pipe mainly because of an initial deflection of the inclined pipe under the gravitational load. It is addressed in a few studies [31,36,37] where the dynamics of the inclined cantilever pipes has been analyzed for the steady or pulsatile internal fluid flow. Although these available studies reveal an indicative effect of the inclination of a pipe on its dynamics, the importance of this geometric parameter (inclination) mainly depends on the rigidity of the pipe. An inclined pipe with high rigidity undergoes a negligibly small initial deflection due to the gravitational load, and thus the corresponding effect on the dynamics of the pipe would not appear in a notable manner. However, in certain applications like heat exchangers, heat pipes and condensers, the inclined pipe may operate under the thermal environment i.e. internal and/or external flow of hot fluid. In these applications, usually a pipe possesses sufficient rigidity to sustain the thermal stresses even though its inclination may yield a notable thermally induced deflection originated from a very small deflection of the inclined pipe under the gravitational load. This high initial deflection would pose certain effects on the dynamic characteristics of an inclined pipe operating under the thermal environment although a corresponding study is not yet reported in the literature to the best knowledge of authors.

However, in this concern of thermal environment or handling the steady or pulsatile flow of hot fluid, the aforesaid FGM may be recommended for the material of the inclined pipe, but the fruitfulness of FGM in this application especially for alleviating the static and dynamic instabilities of the inclined FG pipe is yet to investigate since a similar study is not available in the literature to the best knowledge of authors. The present theoretical work is in this direction where the nonlinear dynamics of a pinned–pinned inclined FG pipe conveying hot fluid with steady or pulsatile flow velocity is investigated thoroughly. Specifically, there are two main objectives of this study. The first one is to investigate the characteristics of divergence (buckling) of the inclined FG pipe on the basis of variations of some system parameters like inclination angle, temperature of fluid and graded material properties of FGM. The second objective is decided as a thorough investigation on the nonlinear dynamics of the inclined FG pipe in association with its divergence on the basis of the variations of the aforesaid system parameters and the material damping of FGM. The overall study is carried out in the following manner.

First, the geometrically nonlinear governing equation of motion of a pinned–pinned inclined FG pipe conveying pulsatile hot fluid is derived. The corresponding nonlinear integral–partial differential equation of motion is converted to the time-differential equation of motion using Galerkin discretization. Subsequently, the incremental harmonic balance (IHB) method and Runge–Kutta method are implemented for evaluation of the nonlinear dynamic responses of the inclined FG pipe in the frequency and time domain, respectively. The local stability of the periodic solutions that are obtained from the IHB method is determined using the Floquet theory whereas the corresponding global stability analysis is conducted by plotting the global bifurcation diagrams. In the numerical results, first, the present formulation and the implementation of the aforesaid solution methodologies are verified. Next, the characteristics of divergence (buckling) of the inclined FG pipe conveying steady hot fluid are investigated based on the variations of inclination angle, temperature and graded material properties of FGM. Subsequently, the nonlinear dynamic responses as well as the corresponding instabilities of the FG pipe are presented. Finally, the effects of material damping of FGM on the dynamic characteristics of the inclined FG pipe are illustrated.

2. System model and governing equation of motion

Fig. 1 shows the schematic diagram of an inclined FG pipe conveying hot fluid with pulsatile flow velocity. The inner and outer cylindrical surfaces of the pipe are considered to be made of ceramic and metal, respectively, and the material properties smoothly vary from inner ceramic rich surface to outer metal rich surface. The ends of the FG pipe are considered as pinned ends, and the hot fluid is assumed to flow with uniform temperature across the ends of the FG pipe. So, the inner ceramic rich surface of the FG pipe is exposed to a high temperature (T_i) while the temperature of the outer metal rich surface of the same pipe is assumed as room temperature ($T_o = 300$ K). For the analysis, the reference Cartesian coordinate system (xyz) is attached to the inclined FG pipe such that the origin of the reference coordinate system lies at the center of the circular cross-section at one end of the pipe. The x-axis is lying along the longitudinal direction of the pipe while the z-axis implies the planar motion of the FG pipe in the xz-plane (Fig. 1). The inclination of longitudinal (x) axis of the FG pipe with the vertical axis is denoted by the angle χ (Fig. 1), and the other geometrical properties like inner radius, outer radius, wall-thickness and length of the FG pipe are symbolized by r_i, r_o, h and L, respectively. Since a slender FG pipe is considered in the present analysis, it is modeled according to the Euler–Bernoulli beam theory. Moreover, the deformations of the pipe are considered to be restricted to long wavelengths as compared to its radius so that the internal flow is modeled according to the plug flow model.

The uniaxial thermo-elastic constitutive relation of FGM can be written in conjunction with the Kelvin–Voigt model [38] as,

$$\sigma_x = \left(E + E^* \frac{\partial}{\partial t}\right)(\varepsilon_x - \alpha_T \Delta T), \Delta T = T(r) - T_o \tag{1}$$

where, σ_x and ε_x are the longitudinal stress and strain, respectively, at any point in the FG pipe; $T(r)$ is the temperature at a radial point (r) within the thickness of the pipe, and T_o is the reference temperature that is considered as the room temperature ($T_o = 300$ K). The material properties of the FG pipe like Young's modulus (E), viscoelastic dissipation parameter(E^*), density(ρ), thermal conductivity (k) and coefficient of thermal expansion(α_T) are the graded properties according to a power law as [39],

$$P(r) = P_m + (P_c - P_m)\left(\frac{1}{2} - \left(\frac{r - r_m}{h}\right)\right)^n \tag{2}$$

where, r_m is the mean radius; P_c and P_m are the properties of ceramic and metal constituents, respectively, and n is the power law exponent or graded exponent. The temperature ($T(r)$) at any radial location (r) within the thickness of the FG pipe can be obtained by solving the one-dimensional steady-state heat conduction equation as,

$$-\frac{1}{r}\frac{\mathrm{d}}{\mathrm{d}r}\left(r\,k(r)\frac{\mathrm{d}T(r)}{\mathrm{d}r}\right) = 0 \text{ with } T = T_o \text{ at } r = r_o \text{ and } T = T_i \text{ at } r = r_i \tag{3}$$

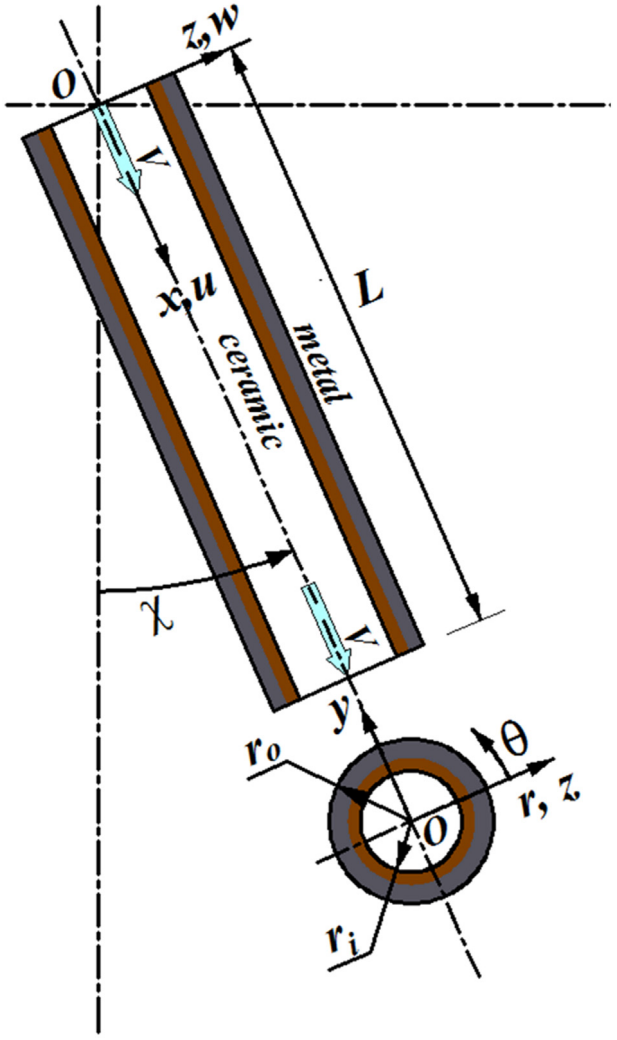

Fig. 1. Schematic diagram of an inclined pinned–pinned FG pipe conveying hot fluid with pulsatile flow velocity.

The solution of Eq. (3) can be obtained as [39],

$$T(r) = T_i + \frac{T_o - T_i}{D_T}\int_{r_i}^{r}\frac{1}{rk(r)}dr, D_T = \int_{r_i}^{r_o}\frac{1}{rk(r)}dr \tag{4}$$

According to Euler–Bernoulli beam theory, the displacements at any point in the FG pipe can be written as,

$$u(x,z,t) = u_0(x,t) - z\frac{\partial w_0(x,t)}{\partial x}, w(x,z,t) = w_0(x,t) \tag{5}$$

where, u_0 and w_0 are the displacements at any point on the middle plane (xy-plane at $z = 0$) of the FG pipe along the x and z directions, respectively. According to this displacement field (Eq. (5)), the von Karman nonlinear strain–displacement relation can be written as,

$$\varepsilon_x = \frac{\partial u_0}{\partial x} + \frac{1}{2}\left(\frac{\partial w_0}{\partial x}\right)^2 - z\frac{\partial^2 w_0}{\partial x^2} \tag{6}$$

The corresponding total potential energy (T_p) of the inclined FG pipe conveying fluid can be written at any instant of time (t) as,

$$\begin{aligned} T_p &= \frac{1}{2}\int_0^L\int_{r_i}^{r_o}\int_0^{2\pi}(\varepsilon_x\sigma_x)r\,dr\,d\theta\,dx - g(m_f+m_p)\\ &\times\int_0^L\langle(x+u)\cos\chi - w\sin\chi\rangle\,dx - \int_0^L T_{in}\left(\frac{\partial u_0}{\partial x} + \frac{1}{2}\left(\frac{\partial w_0}{\partial x}\right)^2\right)dx,\\ m_f &= \rho_f\left(\pi r_i^2\right), m_p = \int_{r_i}^{r_o}\int_0^{2\pi}\rho(r)rdrd\theta, T_{in} = \pi r_i^2 P_{in}(1-2\nu) \end{aligned} \tag{7}$$

where, ρ_f is the mass density of the fluid; g is the acceleration due to gravity; m_f/m_p is the mass per unit length of the fluid/pipe; T_{in} is the axial compressive force per unit length of the pipe due to the internal pressure (P_{in}) of the fluid. In the Eq. (7) and also in the subsequent equations, the subscripts p and f indicate the terms related to the material of the pipe and fluid, respectively. Substituting Eqs. (1) and (6) in Eq. (7), the following expression for the total potential energy (T_p) of the FG pipe conveying fluid can be obtained,

$$\begin{aligned} T_p &= \tfrac{1}{2}\int_0^L\left[\left(D_p + D_p^*\tfrac{\partial}{\partial t}\right)\left(\tfrac{\partial^2 w_0}{\partial x^2}\right)^2\right.\\ &+\left(A_p + A_p^*\tfrac{\partial}{\partial t}\right)\left(\tfrac{\partial u_0}{\partial x} + \tfrac{1}{2}\left(\tfrac{\partial w_0}{\partial x}\right)^2\right)^2\\ &\left.-\left(T_{th}+T_{in}\right)\left(\tfrac{\partial u_0}{\partial x} + \tfrac{1}{2}\left(\tfrac{\partial w_0}{\partial x}\right)^2\right)\right]dx\\ &-g(m_f+m_p)\int_0^L((x+u)\cos\chi - w\sin\chi)dx,\\ D_p &= \int_0^{2\pi}\int_{r_i}^{r_o} z^2E(r)r\,dr\,d\theta, D_p^* = \int_0^{2\pi}\int_{r_i}^{r_o} z^2E^*(r)r\,dr\,d\theta,\\ A_p &= \int_0^{2\pi}\int_{r_i}^{r_o} E(r)rdrd\theta, A_p^* = \int_0^{2\pi}\int_{r_i}^{r_o} E^*(r)rdrd\theta,\\ T_{th} &= \int_0^{2\pi}\int_{r_i}^{r_o} E(r)\alpha_T(r)\Delta T\,rdrd\theta, z = r\sin\theta \end{aligned} \tag{8}$$

where, ν is the Poisson's ratio for the material of the pipe; Tth is the thermally induced force per unit length of the pipe; D_p/A_p is the flexural/axial stiffness per unit length of the pipe while D_p^*/A_p^* are the similar terms related to the energy dissipation from the pipe. The total kinetic energy (T_t) of the FG pipe conveying fluid with a flow velocity V can be expressed as,

$$\begin{aligned} T_t &= \frac{1}{2}m_f\int_0^L\left[\left(V + \frac{\partial u_0}{\partial t} + V\frac{\partial u_0}{\partial x}\right)^2 + \left(\frac{\partial w_0}{\partial t} + V\frac{\partial w_0}{\partial x}\right)^2\right]dx\\ &+\frac{1}{2}m_p\int_0^L\left[\left(\frac{\partial u_0}{\partial t}\right)^2 + \left(\frac{\partial w_0}{\partial t}\right)^2\right]dx \end{aligned} \tag{9}$$

The governing differential equation of motion of the FG pipe conveying fluid is derived employing the extended Hamilton's principle as given by Eq. (10), where δ is an operator for first variation. Substituting Eqs. (8)–(9) in Eq. (10), two coupled governing differential equations of motion of the overall pipe can be obtained for the arbitrary variations of δu_o and δw_o. Presently, the longitudinal inertia force of FG pipe is ignored for its very small magnitude in comparison to that of the transverse inertia force, and the two coupled governing equations of motion are reduced into one equation in terms of the transverse displacement (w_o) following the same procedure as given in [40,41]. The resulting governing equation of motion of the overall FG pipe can be obtained as given in Eq. (11).

$$\int_{t_1}^{t_2}\left(\delta T_t - \delta T_p\right)dt = 0 \tag{10}$$

$$\begin{aligned} &(m_f+m_p)\tfrac{\partial^2 w_0}{\partial t^2} + D_p^*\tfrac{\partial^5 w_0}{\partial x^4\partial t} + 2m_fV\tfrac{\partial^2 w_0}{\partial x\partial t} + D_p\tfrac{\partial^4 w_0}{\partial x^4}\\ &+\left[m_fV^2 + \left(m_f\tfrac{\partial V}{\partial t} - (m_f+m_p)g\cos\chi\right)(L-x) + \right.\\ &\left.T_{th} + T_{in} - \tfrac{A_p}{2L}\int_0^L\left(\tfrac{\partial w_0}{\partial x}\right)^2dx - \tfrac{A_p^*}{L}\int_0^L\left(\tfrac{\partial w_0}{\partial x}\tfrac{\partial^2 w_0}{\partial x\partial t}\right)dx\right]\\ &\tfrac{\partial^2 w_0}{\partial x^2} + (m_f+m_p)g\cos\chi\tfrac{\partial w_0}{\partial x} + (m_f+m_p)g\sin\chi = 0 \end{aligned} \tag{11}$$

The velocity of fluid for pulsatile flow can be expressed as [15],

$$V = V_f(1 + \lambda\cos(\omega t)) \tag{12}$$

where, V_f, λ and ω are the mean flow velocity, pulsation velocity–amplitude and pulsation frequency, respectively. For expressing the governing equation of motion (Eq. (11)) in the dimensionless form, the following dimensionless quantities (Eq. (13)) are introduced where the properties of the metal constituent of the FG pipe at room temperature are considered as the reference material properties that are indicated

by the subscript m.

$$\eta = \frac{w_0}{L}, \xi = \frac{x}{L}, \bar{t} = \left(\frac{D_m}{m_m + m_f}\right)^{1/2} \frac{t}{L^2}, v = \left(\frac{m_f}{D_m}\right)^{1/2} VL,$$
$$\gamma = \frac{m_m + m_f}{D_m} gL^3, \beta = \frac{m_f}{m_m + m_f}, k_m = \frac{AL^2}{2I},$$
$$\alpha = \left(\frac{I}{E_m(m_m + m_f)}\right)^{1/2} \frac{E_m^*}{L^2}, \ \Omega = \left(\frac{m_m + m_f}{D_m}\right)^{1/2} L^2\omega,$$
$$e_T = E_m A \alpha_T (T_i - T_R) L^2/D_m,$$
$$\overline{T}_{in} = T_{in} L^2/D_m \tag{13}$$

In Eq. (13), A and I denote the cross-sectional area of the FG pipe and the area moment of inertia of the same about the y-axis. Introducing the dimensionless quantities (Eq. (13)) in the governing equation of motion (Eq. (11)), the following dimensionless equation of motion can be obtained where the superscript ($'$) or ($\cdot$) denotes the differentiation with respect to ξ or $\bar{t}$.

$$M_1\ddot{\eta} + C_1\dot{\eta}'''' + C_2\dot{\eta}' + K_1\eta'''' + \left[K_2 - K_3 + K_5(1-\xi)\right]\eta'' + K_4\eta' + P_s = 0,$$
$$M_1 = \left\langle \beta + (1-\beta)\overline{m}_p \right\rangle, C_1 = \left\langle \overline{D}_p^* \alpha \right\rangle, C_2 = \left\langle 2\sqrt{\beta}\, v \right\rangle, K_1 = \overline{D}_p,$$
$$K_2 = \left\langle v^2 + \overline{T}_{th}\, e_T + \overline{T}_{in} \right\rangle,$$
$$K_3 = \left\langle \overline{A}_p\, k_m \int_0^1 (\eta')^2 d\xi + 2\overline{A}_p^* k_m \alpha \int_0^1 \eta'\dot{\eta}' d\xi \right\rangle,$$
$$K_4 = \left\langle \gamma \cos\chi \left[\beta + (1-\beta)\overline{m}_p\right] \right\rangle, K_5 = \left\langle \sqrt{\beta}\dot{v} - K_4 \right\rangle,$$
$$P_s = \gamma \sin\chi, \overline{D}_p = D_p/D_m, \overline{D}_p^* = D_p^*/D_m^*, \overline{A}_p = A_p/A_m,$$
$$\overline{A}_p^* = A_p^*/A_m^*, \overline{m}_p = m_p/m_m,$$
$$\overline{T}_{th} = T_{th}/(T_{th})_m \tag{14}$$

3. Solution method

The dimensionless governing equation of motion (Eq. (14)) is solved using the Galerkin method where the basis functions (ϕ_i) are taken as the eigen functions of a pinned–pinned beam. Accordingly, the dimensionless transverse displacement ($\eta(\xi, \bar{t})$) at any point of the FG pipe can be expressed in terms of a number (N) of basis functions and the associated generalized coordinates (q_i) as,

$$\eta(\xi, \bar{t}) = \sum_{i=1}^{N} \phi_i(\xi) q_i(\bar{t}) = \boldsymbol{\Phi}\, \boldsymbol{q} \tag{15}$$

where, $\boldsymbol{\Phi}$ and $\boldsymbol{q}$ are the vectors of basis functions and generalized coordinates, respectively. Substituting Eq. (15) in the Eq. (14), the discretized governing equation of motion of the FG pipe conveying hot fluid with pulsatile flow velocity can be obtained as,

$$\boldsymbol{M}\,\ddot{\boldsymbol{q}} + \boldsymbol{G}(\Omega, \lambda, \bar{t})\dot{\boldsymbol{q}} + \boldsymbol{K}(\Omega, \lambda, \bar{t})\boldsymbol{q} + 2\overline{A}_p^* k_m \alpha(\boldsymbol{q}^{\mathrm{T}}\boldsymbol{C}\,\dot{\boldsymbol{q}})\boldsymbol{C}\,\boldsymbol{q} + \overline{A}_p k_m (\boldsymbol{q}^{\mathrm{T}}\boldsymbol{C}\,\boldsymbol{q})\boldsymbol{C}\,\boldsymbol{q} + P_s\boldsymbol{F} = 0,$$
$$\boldsymbol{M} = M_1\boldsymbol{I}, \boldsymbol{G} = C_1\boldsymbol{\Lambda} + C_2\boldsymbol{B}, \boldsymbol{K} = \langle K_1\boldsymbol{\Lambda} + K_2\boldsymbol{C} + K_5(\boldsymbol{C} - \boldsymbol{D}) + K_4\boldsymbol{B}\rangle,$$
$$\boldsymbol{\Lambda} = \int_0^1 \boldsymbol{\Phi}^{\mathrm{T}}\boldsymbol{\Phi}''''\, d\xi, \boldsymbol{B} = \int_0^1 \boldsymbol{\Phi}^{\mathrm{T}}\boldsymbol{\Phi}'\, d\xi, \boldsymbol{C} = \int_0^1 \boldsymbol{\Phi}^{\mathrm{T}}\boldsymbol{\Phi}''\, d\xi,$$
$$\boldsymbol{D} = \int_0^1 \xi\,\boldsymbol{\Phi}^{\mathrm{T}}\boldsymbol{\Phi}''\, d\xi, \boldsymbol{F} = \int_0^1 \boldsymbol{\Phi}^{\mathrm{T}} d\xi \tag{16a}$$

In Eq. (16a), $\boldsymbol{I}$ is the unity matrix and the elements of $\boldsymbol{\Lambda}$, $\boldsymbol{B}$, $\boldsymbol{C}$, $\boldsymbol{D}$ and $\boldsymbol{F}$ are given in Eq. (16b) where λ_i denotes the ith eigen value corresponding to the basis function ϕ_i.

$$I_{ij} = \begin{cases} 0 & i \neq j \\ 1 & i = j \end{cases}, \Lambda_{ij} = \begin{cases} 0 & i \neq j \\ \lambda_i^4 & i = j \end{cases}, B_{ij} = \begin{cases} \frac{2\langle -1 + (-1)^{i+j}\rangle \lambda_i \lambda_j}{\lambda_j^2 - \lambda_i^2} & i \neq j \\ 0 & i = j \end{cases},$$
$$C_{ij} = \begin{cases} 0 & i \neq j \\ -\lambda_i^2 & i = j \end{cases}, D_{ij} = \begin{cases} \frac{4\langle 1 - (-1)^{i+j}\rangle \lambda_j^3 \lambda_i}{(\lambda_i^2 - \lambda_j^2)^2} & i \neq j \\ 0.5 C_{ij} & i = j \end{cases},$$
$$F_i = \sqrt{2}\left\langle 1 - (-1)^i \right\rangle / \lambda_i, where\ i, j = 1, 2, 3....N \tag{16b}$$

The nonlinear time-differential equation of motion (Eq. (16a)) of the FG pipe is solved using the incremental harmonic balanced (IHB) method. A pipe conveying pulsatile fluid is usually subjected to the parametric resonance at the frequency of $2\ \Omega_n/i$ [1], where Ω_n ($n = 1, 2, 3, \ldots$) is the natural frequency and i is a positive integer. So, the solution ($\boldsymbol{q}$) of the differential equation (Eq. (16a)) is assumed following the Fourier series with the finite number (H) of harmonics as,

$$\boldsymbol{q} = \boldsymbol{q}^0 + \sum_{i=1}^{H} \left\langle \boldsymbol{q}_i^c \cos(i\,\Omega\bar{t}/2) + \boldsymbol{q}_i^s \sin(i\,\Omega\bar{t}/2) \right\rangle \tag{17}$$

where, $\boldsymbol{q}^0$, $\boldsymbol{q}_i^c$, $\boldsymbol{q}_i^s$ are the Fourier coefficient vectors corresponds to constant, cosine and sine terms, respectively. For the convenience of formulation, $\Omega/2$ is represented by $\overline{\Omega}$, and also the differential equation (Eq. (16a)) is expressed in terms of τ by substituting $\tau = \overline{\Omega}\bar{t}$. Accordingly, Eqs. (17) and (16a) can be written in a compact form as,

$$\boldsymbol{q} = \boldsymbol{S}\,\boldsymbol{X},$$
$$\boldsymbol{S} = \boldsymbol{Q} \otimes \boldsymbol{I}_{N\times N}, \boldsymbol{Q} = \left\{1\boldsymbol{Q}_c \ \ \boldsymbol{Q}_s\right\}, \boldsymbol{Q}_c = \{\cos\tau \ \ \cos 2\tau \ \ \ldots \ \ \cos \mathrm{H}\tau\},$$
$$\boldsymbol{Q}_s = \{\sin\tau \ \ \sin 2\tau \ \ \ldots \ \ \sin \mathrm{H}\tau\}$$
$$\boldsymbol{X} = \left\{(\boldsymbol{q}^0)^{\mathrm{T}}(\boldsymbol{q}^c)^{\mathrm{T}}(\boldsymbol{q}^s)^{\mathrm{T}}\right\}^{\mathrm{T}} \tag{18}$$
$$\overline{\Omega}^2\boldsymbol{M}\,\ddot{\boldsymbol{q}} + \boldsymbol{K}(\overline{\Omega}, \lambda, \tau)\boldsymbol{q} + \overline{\Omega}\boldsymbol{G}(\lambda, \tau)\dot{\boldsymbol{q}}0 + 2\overline{A}_p^* k_m \alpha\, \overline{\Omega}(\boldsymbol{q}^{\mathrm{T}}\boldsymbol{C}\,\dot{\boldsymbol{q}})\boldsymbol{C}\,\boldsymbol{q} + \overline{A}_p k_m (\boldsymbol{q}^{\mathrm{T}}\boldsymbol{C}\,\boldsymbol{q})\boldsymbol{C}\,\boldsymbol{q} + P_s\boldsymbol{F} = 0 \tag{19}$$

where, $\boldsymbol{I}_{N\times N}$ is the unity matrix of size $N \times N$ and $\otimes$ is the Kronecker product.

In order to obtain the linearized incremental governing equation of motion, the state variables ($\boldsymbol{q}$, $\overline{\Omega}$, λ) are first taken in an incremental form ($\boldsymbol{q} = \boldsymbol{q}_0 + \Delta\boldsymbol{q}\ \overline{\Omega} = \overline{\Omega}_0 + \Delta\overline{\Omega}, \lambda = \lambda_0 + \Delta\lambda$) about a reference state ($\boldsymbol{q}_0$, $\overline{\Omega}_0$, λ_0) of vibration. Subsequently, the governing differential equation of motion (Eq. (19)) is modified keeping the linear incremental terms only as given in Eq. (20).

$$\overline{\Omega}_0^2\boldsymbol{M}\,\Delta\ddot{\boldsymbol{q}} + \overline{\boldsymbol{R}}_G\,\Delta\dot{\boldsymbol{q}} + \overline{\boldsymbol{R}}_K\,\Delta\boldsymbol{q} = \overline{\boldsymbol{R}} - \overline{\boldsymbol{R}}_{\overline{\Omega}}\Delta\overline{\Omega} - \overline{\boldsymbol{R}}_\lambda\,\Delta\lambda,$$
$$\overline{\boldsymbol{R}}_K = \boldsymbol{K}(\overline{\Omega}_0, \lambda_0, \tau) + \overline{A}_p\, k_m \left\langle (\boldsymbol{q}_0)^{\mathrm{T}}\boldsymbol{C}\,\boldsymbol{q}_0\boldsymbol{C} + 2\boldsymbol{C}\,\boldsymbol{q}_0(\boldsymbol{q}_0)^{\mathrm{T}}\boldsymbol{C} \right\rangle + 2\overline{A}_p^* k_m \alpha\, \overline{\Omega}_0 \left\langle (\boldsymbol{q}_0)^{\mathrm{T}}\boldsymbol{C}\,\dot{\boldsymbol{q}}_0\boldsymbol{C} + \boldsymbol{C}\,\boldsymbol{q}_0(\dot{\boldsymbol{q}}_0)^{\mathrm{T}}\boldsymbol{C} \right\rangle,$$
$$\overline{\boldsymbol{R}}_G = \overline{\Omega}_0\boldsymbol{G}(\lambda_0, \tau) + 2\overline{A}_p^* k_m \alpha\, \overline{\Omega}_0\boldsymbol{C}\,\boldsymbol{q}_0(\boldsymbol{q}_0)^{\mathrm{T}}\boldsymbol{C},$$
$$\overline{\boldsymbol{R}}_\lambda = 2\sqrt{\beta}v_f \cos 2\tau\ \boldsymbol{B}\,\dot{\boldsymbol{q}}_0 + 2v\, v_f \cos 2\tau\ \boldsymbol{C}\,\boldsymbol{q} - 2\sqrt{\beta}\, v_f \overline{\Omega}_0 \sin 2\tau(\boldsymbol{C} - \boldsymbol{D})\boldsymbol{q}_0,$$
$$\overline{\boldsymbol{R}}_{\overline{\Omega}} = \boldsymbol{G}(\lambda_0, \tau)\dot{\boldsymbol{q}}_0 - 2\sqrt{\beta}v_f\lambda_0 \sin 2\tau(\boldsymbol{C} - \boldsymbol{D})\boldsymbol{q}_0 + 2\overline{\Omega}_0\boldsymbol{M}\,\ddot{\boldsymbol{q}}_0 + 2\overline{A}_b^* k_m \alpha(\boldsymbol{q}_0)^{\mathrm{T}}\boldsymbol{C}\,\dot{\boldsymbol{q}}_0\boldsymbol{C}\,\boldsymbol{q}_0,$$
$$\overline{\boldsymbol{R}} = P_s\,\boldsymbol{F} - \left(\overline{\Omega}_0^2\boldsymbol{M}\,\ddot{\boldsymbol{q}}_0 + \boldsymbol{K}(\overline{\Omega}_0, \lambda_0, \tau)\boldsymbol{q}_0 + \overline{\Omega}_0\boldsymbol{G}(\lambda_0, \tau)\dot{\boldsymbol{q}}_0 + \overline{A}_p\, k_m(\boldsymbol{q}_0)^{\mathrm{T}}\boldsymbol{C}\,\boldsymbol{q}_0\boldsymbol{C}\,\boldsymbol{q}_0 + 2\overline{A}_p^* k_m \alpha\, \overline{\Omega}_0(\boldsymbol{q}_0)^{\mathrm{T}}\boldsymbol{C}\,\dot{\boldsymbol{q}}_0\boldsymbol{C}\,\boldsymbol{q}_0\right) \tag{20}$$

For expressing the linearized incremental governing equation of motion (Eq. (20)) in the frequency-domain, the Galerkin procedure is utilized with the assumed periodic solution (Eq. (18)), and the resulting equation is obtained as,

$$\boldsymbol{K}_J\,\Delta\boldsymbol{X} = \boldsymbol{R} - \boldsymbol{R}_{\overline{\Omega}}\Delta\overline{\Omega} - \boldsymbol{R}_\lambda\,\Delta\lambda,$$
$$\boldsymbol{K}_J = \int_0^{2\pi} \boldsymbol{S}^{\mathrm{T}}\left(\overline{\Omega}_0^2\boldsymbol{M}\,\ddot{\boldsymbol{S}} + \overline{\boldsymbol{R}}_G\,\dot{\boldsymbol{S}} + \overline{\boldsymbol{R}}_K\,\boldsymbol{S}\right) d\tau, \boldsymbol{R} = \int_0^{2\pi} \boldsymbol{S}^{\mathrm{T}}\overline{\boldsymbol{R}} d\tau,$$
$$\boldsymbol{R}_{\overline{\Omega}} = \int_0^{2\pi} \boldsymbol{S}^{\mathrm{T}}\overline{\boldsymbol{R}}_{\overline{\Omega}} d\tau, \boldsymbol{R}_\lambda = \int_0^{2\pi} \boldsymbol{S}^{\mathrm{T}}\overline{\boldsymbol{R}}_\lambda\, d\tau \tag{21}$$

The solution of Eq. (21) within a range of frequency of pulsatile fluid flow provides the frequency response curve of the overall FG pipe.

4. Local stability analysis

The local stability of a steady-state nonlinear response can be determined by imposing a small perturbation to it (response). The substitution of this perturbation ($\boldsymbol{q} = \boldsymbol{q}_0 + \Delta\boldsymbol{q}$) in Eq. (19) yields the following expression that is similar to Eq. (20).

$$\overline{\Omega}_0^2 \boldsymbol{M}\,\Delta\ddot{\boldsymbol{q}} + \overline{\boldsymbol{R}}_G\,\Delta\dot{\boldsymbol{q}} + \overline{\boldsymbol{R}}_K\,\Delta\boldsymbol{q} = \overline{\boldsymbol{R}} \tag{22}$$

where, the steady-state solution ($\boldsymbol{q}_0$) satisfies the governing equation of motion (Eq. (19)) for which $\overline{\boldsymbol{R}} = 0$. Eq. (22) is a second order linear time differential equation (in terms of $\Delta\boldsymbol{q}$) with periodic coefficients, and thus the stability of the nonlinear response can be obtained using Floquet theory by expressing the differential equation (Eq. (22)) in the state-space form as,

$$\dot{\boldsymbol{F}} = \boldsymbol{Q}_t(\tau)\boldsymbol{F}, \boldsymbol{F} = \{\Delta\boldsymbol{q}\ \ \Delta\dot{\boldsymbol{q}}\}^{\mathrm{T}}, \boldsymbol{Q}_t(\tau) = \begin{bmatrix} \boldsymbol{0} & \boldsymbol{I} \\ -\frac{1}{\overline{\Omega}_o^2}\boldsymbol{M}^{-1}\overline{\boldsymbol{R}}_K & -\frac{1}{\overline{\Omega}_o^2}\boldsymbol{M}^{-1}\overline{\boldsymbol{R}}_G \end{bmatrix} \tag{23}$$

The stability characteristics of solution can be obtained from the eigen values of the state transition matrix ($\boldsymbol{\Psi}$) satisfying $\boldsymbol{F}(\tau + T_m) = \boldsymbol{\Psi}\ \boldsymbol{F}(\tau)$, where T_m is the time period (2π) of the system (Eq. (23)). If all the moduli of eigen values of $\boldsymbol{\Psi}$ are less than 1 then the solution will be stable, otherwise it is unstable. Presently, this state transition matrix ($\boldsymbol{\Psi}$) is computed following a procedure proposed by Friedmann et al. [42], where the transition matrix is evaluated using fourth order Runge–Kutta method and Gill coefficients according to the following expressions,

$$\begin{aligned}
\boldsymbol{\Psi} &= \sum_{i=1}^{N_t} \boldsymbol{K}_t(T_m - i\,\Delta\tau), \\
\boldsymbol{K}_t(\tau) &= \boldsymbol{I} + \frac{\Delta\tau}{6}\left(\boldsymbol{Q}_t(\tau) + 2\left(1 - \frac{1}{\sqrt{2}}\right)\boldsymbol{E}_t(\tau)\right. \\
&\quad \left. + 2\left(1 + \frac{1}{\sqrt{2}}\right)\boldsymbol{F}_t(\tau) + \boldsymbol{G}_t(\tau)\right), \\
\boldsymbol{F}_t(\tau) &= \left[\boldsymbol{Q}_t\left(\tau + \frac{\Delta\tau}{2}\right)\right]\left(\boldsymbol{I} + \left(-\frac{1}{2} + \frac{1}{\sqrt{2}}\right)\Delta\tau\,\boldsymbol{Q}_t(\tau)\right. \\
&\quad \left. + \left(1 - \frac{1}{\sqrt{2}}\right)\Delta\tau\,\boldsymbol{E}_t(\tau)\right), \\
\boldsymbol{G}_t(\tau) &= \left[\boldsymbol{Q}_t(\tau + \Delta\tau)\right]\left(\boldsymbol{I} - \frac{\Delta\tau}{\sqrt{2}}\boldsymbol{E}_t(\tau) + \left(1 + \frac{1}{\sqrt{2}}\right)\Delta\tau\,\boldsymbol{F}_t(\tau)\right), \\
\boldsymbol{E}_t(\tau) &= \left[\boldsymbol{Q}_t\left(\tau + \frac{\Delta\tau}{2}\right)\right]\left(\boldsymbol{I} + \frac{1}{2}\Delta\tau\,\boldsymbol{Q}_t(\tau)\right)
\end{aligned} \tag{24}$$

In Eq. (24), N_t is the number of time steps; $\Delta\tau\ \left(= T_m/N_t\right)$ is the time step of the Runge–Kutta numerical integration.

5. Results and discussions

In this section, the numerical results are presented to investigate the nonlinear static and dynamic responses of the inclined FG pipe conveying steady or pulsatile hot fluid. The geometrical properties of the pipe are taken as, $r_i = 12$ mm, $r_o = 13.5$ mm, $L = 2$ m. The density of the fluid is considered as 990 kg/m^3 while it (fluid) flows through the FG pipe with an internal pressure of 4.4 MPa above the atmospheric pressure. The temperature dependent material properties of the metal (Ti-6Al-4V) and ceramic (ZrO_2) constituents of FG material are given in Eqs. (25) and (26), respectively [43,44]. The material damping of FGM is considered through its metal constituent only, where the coefficient of viscoelastic dissipation parameter or retardation time (r_τ) is considered as 0.0004 s [45] corresponding to the dissipation parameter ($E^* = r_\tau\,E$) for the metal constituent. With these properties of the constituent materials, the properties at any point in the FG pipe can be determined according to Eq. (2) where the temperature-dependent properties of the constituents can be computed from Eqs. (25) and (26) in conjunction with the solution for temperature distribution (Eq. (4)) across the wall-thickness the pipe. The Poisson's ratio of FGM is assumed to be constant with the value of 0.3.

$$\begin{aligned}
&E(T) = (122.14 - 0.055T)\ \text{GPa}, \\
&\alpha_T(T) = (7.2347 - 0.0071277T - 5.2876\times10^{-6}T^2 \\
&\quad + 1.2697\times10^{-9})\times10^{-6}\ \text{K}^{-1}, \\
&k = 7.8\ \text{Wm}^{-1}\text{K}^{-1}, \rho = 4429\ \text{Kgm}^{-3}
\end{aligned} \tag{25}$$

$$\begin{aligned}
&E(T) = (235.38 - 0.30377T + 2.6734\times10^{-4}T^2 - 8.17\times10^{-8}T^3)\ \text{GPa}, \\
&\alpha(T) = (13.628 - 0.018913T + 1.2413\times10^{-5}T^2)\times10^{-6}\ \text{K}^{-1}, \\
&k = 1.8\ \text{Wm}^{-1}\text{K}^{-1}, \rho = 3000\ \text{Kgm}^{-3}
\end{aligned} \tag{26}$$

The static/dynamic responses of the inclined FG pipe are illustrated on the basis of the variations of the system parameters like inner surface temperature (T_i), graded exponent (n), inclination angle (χ), mean flow velocity (V_f) and pulsation amplitude (λ). The static responses are evaluated by solving Eq. (16a) without consideration of the time-dependent terms, whereas the dynamic responses in the frequency domain are evaluated by solving Eq. (21) in conjunction with the arc-length extrapolation continuation method [46]. The dynamic responses of the FG pipe in the time-domain are evaluated by solving Eq. (16a) using the adaptive Runge–Kutta method especially for the clarification of dynamics of the inclined FG pipe through the global bifurcation diagram where the Poincare sections are selected based on the time-period ($2\pi/\Omega$) of the excitation frequency (Ω). In all the following numerical results, the responses (η) of the inclined FG pipe is presented corresponding to its middle point ($\xi = 0.5$), and it is denoted by η_m.

Since the present mathematical model of the inclined FG pipe is derived based on the Galerkin discretization and IHBM, a convergence study is first carried out where the nonlinear frequency responses of the FG pipe are evaluated by a gradual increase of the number of basis functions in the Galerkin discretization as well as the number of harmonic terms in IHBM. It is observed that the results appear with the sufficient numerical accuracy for the first seven basis functions (Eq. (15), $N = 7$) in the Galerkin discretization and first six harmonic terms (Eq. (17), $H = 6$) in IHBM, and thus the same are considered in the present numerical results.

5.1. Verification of present formulation

In order to verify the present formulation for handling the thermo-elastic coupling in the FG pipe, its metal and ceramic constituents are considered as SUS304 and Si_3N_4, respectively, while the FG pipe is taken in vertical orientation ($\chi = 0$) without any fluid flow. Under these conditions, the critical buckling temperature is computed for uniform temperature across the wall-thickness of the FG pipe. These results are illustrated in Table 1 for both the temperature-independent and temperature-dependent properties of the constituent materials. Similar results for an identical FG pipe are available in [47], and the same are also furnished in Table 1. It may be observed from Table 1 that the present results are in good agreement with the similar results available in [47] thus verifying the present formulation in handling the thermo-elastic coupling in the FG pipe.

The results for nonlinear dynamic response of an inclined FG pipe are not available in the literature, and thus the present formulation in modeling an inclined pipe is verified following the available results in [48] for static profile of an inclined submerged pinned–pinned isotropic pipe under an externally applied tensile force. Here, the present governing equation (Eq. (11)) is modified slightly by adding the terms corresponding to the applied tensile force (T_e) and the added mass (m_e) for external fluid (submerged) as presented in Eq. (27), and the computed static profile of the inclined isotropic pipe at room temperature is plotted in Fig. 2a together with the similar results in [48].

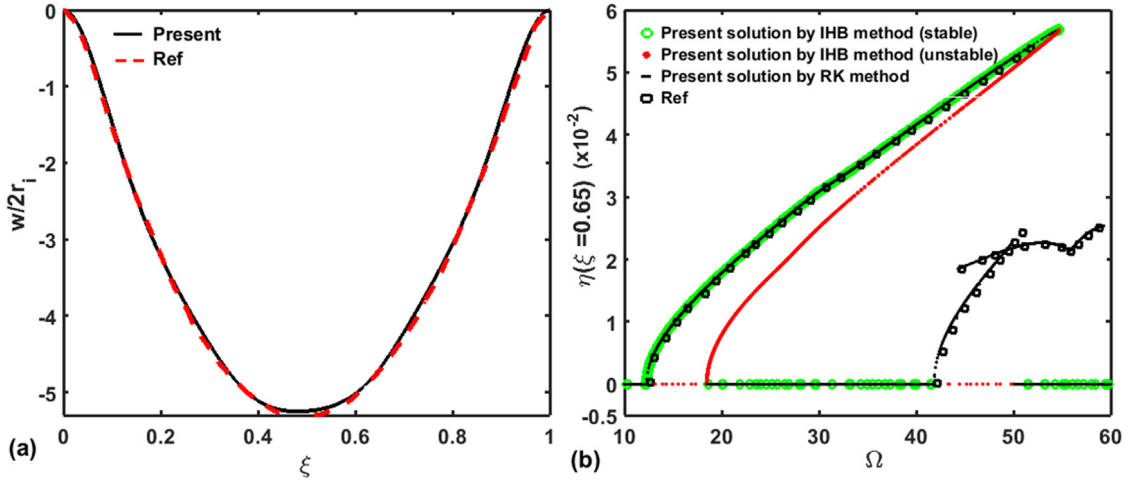

Fig. 2. (a) Comparison of the static profile of an inclined isotropic pipe with that for an identical pipe in Ref. [48], (b) comparison of nonlinear dynamic response of vertical isotropic pipe conveying pulsatile fluid with the similar response of an identical pipe in Ref. [15]. (RK: Runge–Kutta).

Table 1
Comparison of critical buckling temperatures of FG pipe ($r_o = 0.5$ mm, $r_i = 0.5r_o$).

Exponent (n)	L/r_o	Temperature dependent		Temperature independent	
		Present	Fu et al. [47]	Present	Fu et al. [47]
∞ (SUS304)	25	273.44	273.43	400.23	400.22
4	25	325.64	325.61	499.74	499.74
2	25	353.21	353.19	551.84	551.84
1	25	384.48	384.46	612.12	612.12
0 (Si_3N_4)	25	489.20	489.20	840.35	840.35

A good agreement of the present results with that in the reference [48] can be observed from Fig. 2a, and this comparison verifies the present formulation in handling the inclined pipes.

$$D_p \frac{\partial^4 w_0}{\partial x^4} + \left[m_f V^2 - T_e - \left\langle (m_f + m_p - m_e) g \cos\chi \right\rangle (L - x) - \frac{A_p}{2L} \int_0^L \left(\frac{\partial w_0}{\partial x} \right)^2 dx \right] \frac{\partial^2 w_0}{\partial x^2} + (m_f + m_p - m_e) g \cos\chi \frac{\partial w_0}{\partial x} + (m_f + m_p - m_e) g \sin\chi = 0 \quad (27)$$

$m_e = \rho_e A_e$, $A_e = \pi r_o^2$

For a verification of the present IHB formulation and implementation of adaptive Runge–Kutta method in evaluation of the nonlinear dynamic responses of the FG pipe, similar results are not available in the literature. However, it is carried out by taking a result in reference [15] for nonlinear dynamic response of a vertically oriented ($\chi = 0$) pinned–pinned isotropic pipe conveying pulsatile fluid. This comparison is illustrated in Fig. 2b, where the present results are evaluated through both the IHB formulation and adaptive Runge–Kutta method. It may be observed from Fig. 2b that the present results are in good agreement with that in reference [15] thus verifying the present IHB formulation, as well as the present implementation of the adaptive Runge–Kutta method, in evaluating the nonlinear dynamic responses of pipes conveying pulsatile fluid.

5.2. Nonlinear response of the inclined FG pipe conveying hot fluid with constant flow velocity

For an inclined pipe, the gravitational load is usually accounted by its two components along the axial and transverse directions to the length of the pipe. The axial component causes a small increase of the axial tension in the pipe, and it lowers the effect of transverse component that causes the transverse deflection of the pipe. However, this initial transverse deflection of the inclined pipe has certain effect on its (pipe) deformation characteristics under the forces associated with the fluid flow [31,35,37,49]. So, first, the transverse deflection of the inclined FG pipe under the gravitational load is evaluated at the room temperature ($T_i = T_o = 300$ K). The corresponding static profiles of the FG pipe are illustrated in Fig. 3a for its different orientation angles (χ) with the vertical axis, where the graded exponent (n) of FGM is taken as 4 and the fluid velocity is assumed as zero ($V_f = 0$). However, the fluid velocity (V_f) is varied subsequently and the corresponding variation of the maximum transverse deflection (η_m) of the inclined FG pipe is illustrated in Fig. 3b for different values of the graded exponent (n) at an inclination angle (χ) of 45^0. It may be observed from Fig. 3a that the maximum transverse deflection appears at the middle span ($\xi \approx 0.5$) of the pipe for its any inclination angle, and this transverse deflection increases for a higher inclination angle of the FG pipe. If the velocity (V_f) of the steady flow of fluid increases, then Fig. 3b shows a very small increase in the maximum transverse deflection (η_m) of the FG pipe due to the induced follower compressive force. The corresponding magnitude of static deflection (η) indicates an insignificant effect of the gravitational force on the static deflection of the inclined FG pipe conveying fluid with constant flow velocity, and it appears mainly due to the high stiffness of the FG pipe. However, a different observation is obtained when the inclined FG pipe conveys hot fluid with constant flow velocity as it is presented in the next result.

A FG pipe conveying hot fluid is susceptible to undergo the divergence instability (buckling) due to the combined effect of thermally induced compressive stress and the similar stress due to the flow velocity. However, the thermally induced stress is significantly higher than the stress induced due to the flow velocity [26], and thus the temperature in the pipe is more important parameter than the steady flow velocity in concern to its (pipe) divergence instability or buckling. So, the influence of temperature of hot fluid on the static (divergence) instability of the inclined FG pipe is first investigated through the results in Fig. 4, where, for different values of the inclination angle (χ) and graded exponent (n) of FGM, the variations of its (FG pipe) maximum transverse deflection (η_m) with the inner wall temperature ($T_i \neq 300$ K, $T_o = 300$ K) are illustrated for a steady flow velocity ($V_f = 5$ m/s). For vertical FG pipe ($\chi = 0$), it may be observed from Fig. 4 that the divergence of the pipe appears through the pitch-fork bifurcation (points P_1 and P_2) at a certain temperature that is called as the critical buckling temperature. The state of the vertical FG pipe arrives at any of the two symmetric buckled equilibriums (positive and negative) beyond the critical buckling temperature where an unstable equilibrium also appears as indicated by the dotted line (blue dotted lines, Fig. 4). However, as the FG pipe becomes inclined one ($\chi \neq 0$), the aforesaid initial transverse deflection of the pipe arises due to the gravitational load, and it causes the buckling of the

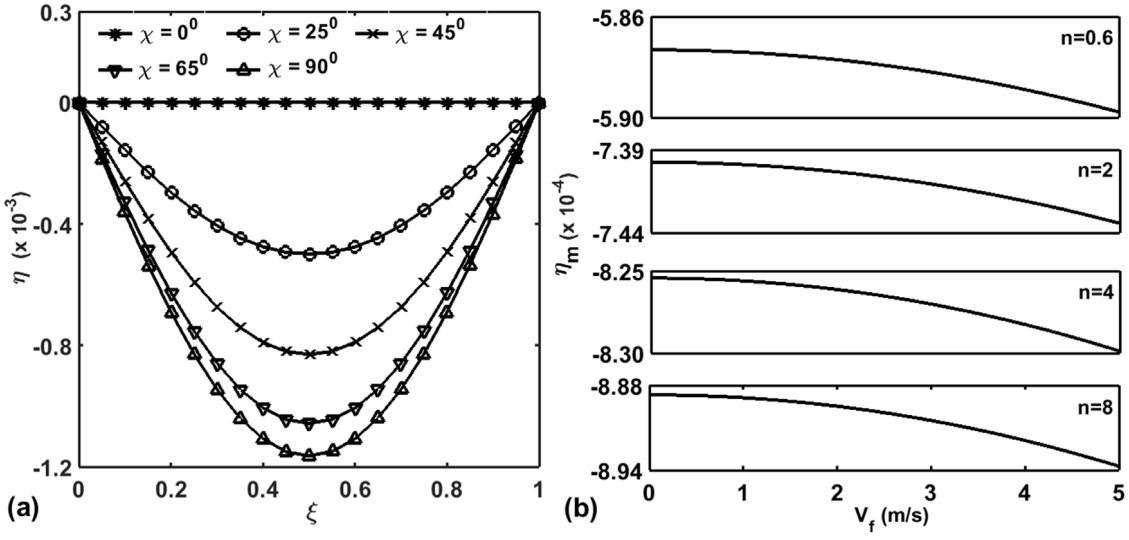

Fig. 3. (a) Variation of static profile of FG pipe ($n = 4$) having the internal mass of fluid ($V_f = 0$) for different values of its (pipe) inclination angle, (b) variation of maximum transverse deflection (η_m) of the inclined FG pipe ($\chi = 45^0$) with the velocity (V_f) of internal steady flow of fluid for different values of the graded exponent (n) of FGM ($T_i = T_o = 300$ K).

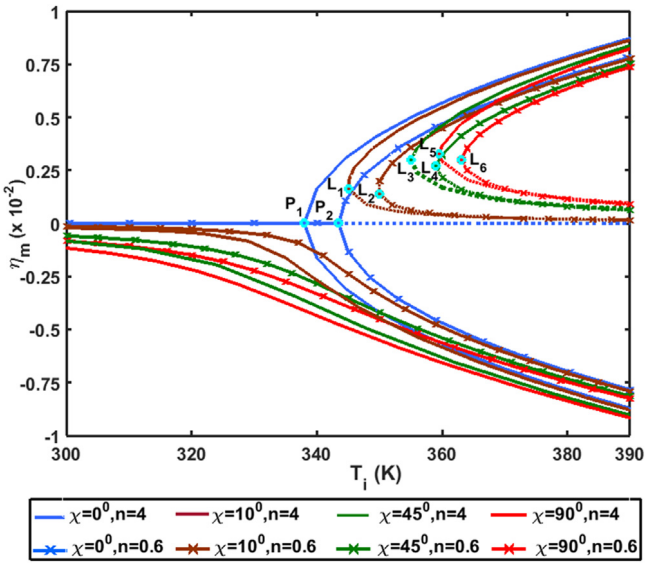

Fig. 4. Variation of maximum transverse deflection (η_m) of the inclined FG pipe with the temperature (T_i) of the internal fluid flow ($V_f = 5$ m/s).

FG pipe through the saddle–node bifurcation (points L_1, L_2, L_3, L_4, L_5, L_6, Fig. 4). The corresponding critical buckling temperature (at saddle–node bifurcation) is indicatively higher than that (at pitchfork bifurcation) for the vertical FG pipe ($\chi = 0$). Beyond the saddle–node bifurcation, the inclined FG pipe arrives at any of the positive and negative stable equilibriums while an unstable equilibrium also appears as it is indicated by the dotted line in Fig. 4. It is important to note from the results in Fig. 4 that a very small inclination of the FG pipe is sufficient to cause its divergence through the saddle–node bifurcation. However, as the angle of inclination increases, the buckling instability occurs at higher temperature while the corresponding critical buckling temperature decreases with the increase of the graded exponent (n) of FGM (Fig. 4).

5.3. Nonlinear dynamic response of inclined FG pipe conveying pulsatile hot fluid

Generally, a pipe conveying pulsatile fluid undergoes dynamic instability by means of the parametric resonance. Depending on the frequency of pulsatile flow and natural frequency of the pipe system, three kinds of parametric resonances (instabilities) namely primary, secondary and combinatory resonances may appear [15]. However, since the present FG pipe possesses high stiffness, it is observed that the combinatory parametric resonance occurs at very high frequency of pulsatile flow, and this frequency of pulsatile flow may not be feasible in practical applications of the FG pipe. So, the results here are presented for the primary and secondary parametric resonances corresponding to the fundamental mode of vibration of the FG pipe as these resonances appear within a feasible range of frequency of pulsatile flow. Now, as discussed in the earlier section, the divergence of the FG pipe yields its two equilibrium states namely pre-buckled and post-buckled equilibrium states. For each of these equilibrium states of the FG pipe, its dynamic instabilities and the associated motion due to pulsatile fluid flow are presently analyzed on the basis of the variations of some system parameters namely temperature (T_i), graded exponent (n) of FGM, mean flow velocity (V_f), pulsation amplitude (λ) and material damping of FGM.

5.3.1. Effect of temperature

Fig. 5a illustrates the frequency response of the vertical FG pipe ($\chi = 0$) at a temperature corresponding to its pre-buckled state. This result shows the appearance of the principal primary parametric resonance at the frequency of 2 Ω_n, where Ω_n is the natural frequency of the vertical FG pipe conveying hot fluid with steady flow velocity ($\lambda = 0$). This resonance evolves through the supercritical and subcritical pitchfork bifurcations ((M) and (N), Fig. 5a). Due to this parametric resonance, the FG pipe undergoes periodic oscillation in its pre-buckled state with respect to the corresponding equilibrium position ($\eta_m = 0$). It should be noted here that the oscillation of the FG pipe at a frequency with reference to an equilibrium position is illustrated (Fig. 5a) by plotting the corresponding maximum and minimum deflections of the pipe as well as the mean point of oscillation. This kind of illustration of motion of the FG pipe is also adopted in the subsequent results for its (FG pipe) frequency responses. It should also be noted here that the red and green points over a response curve indicate the unstable and stable dynamic responses of the FG pipe, respectively. The kind of bifurcation

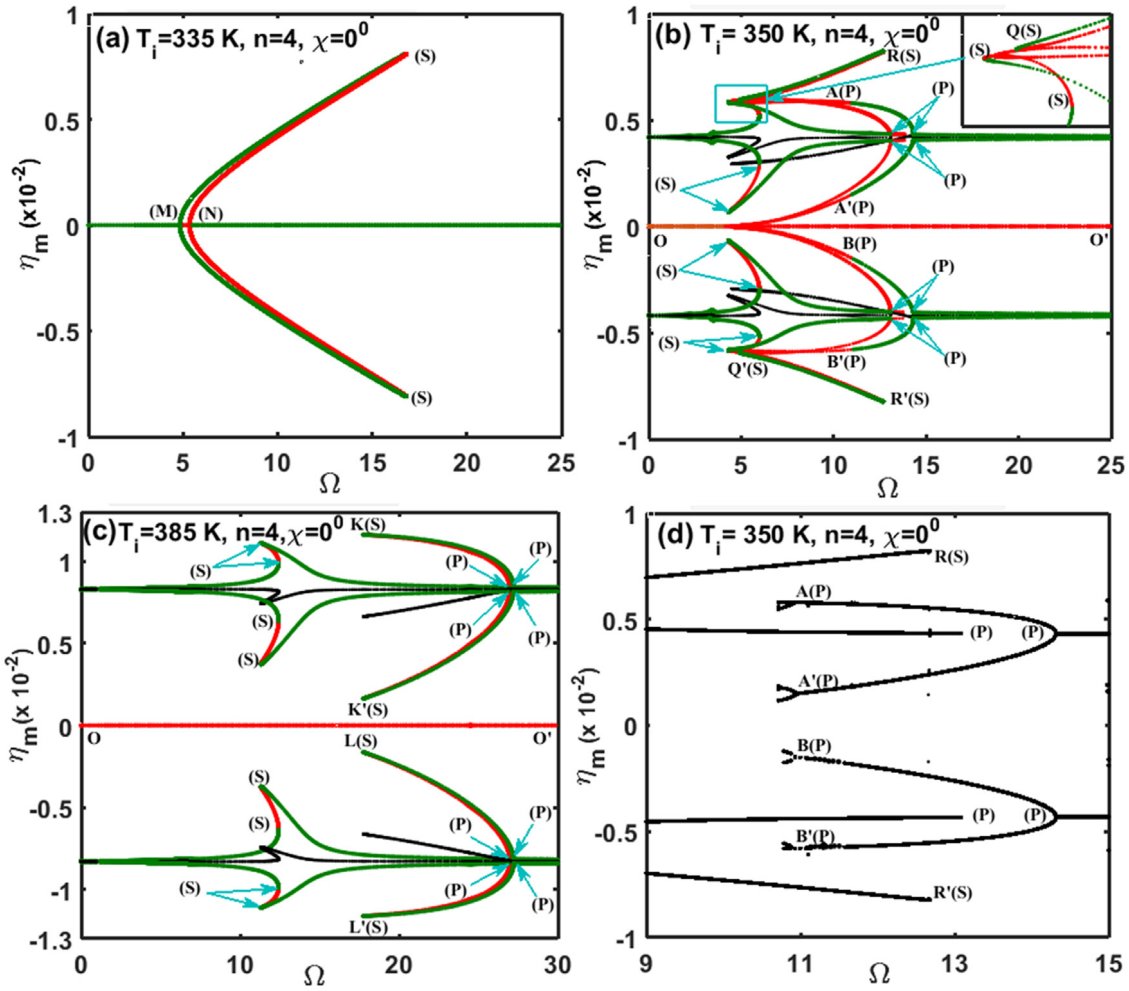

Fig. 5. Nonlinear frequency responses of the vertical FG pipe ($\chi = 0$) at its (a) pre-buckled state (T_i = 335 K) and (b)–(c) post-buckled state (T_i = 350 K, 385 K), (d) global bifurcation diagram with respect to pulsation frequency at the neighborhood of bifurcation points A/A′ and B/B′ in Fig. 5b ($n = 4$, $V_f = 5$ m/s and $\lambda = 0.5$). (For interpretation of the references to color in this figure legend, the reader is referred to the web version of this article.)

at a point on the frequency response curve is identified by computing the Floquet multipliers, where it is observed from the present results that four kinds of bifurcations namely supercritical pitchfork, subcritical pitchfork, saddle–node and period doubling/period demultiplying bifurcations appear, and the same are denoted over the corresponding points of a response curve by (M), (N), (S) and (P), respectively.

Fig. 5b–c illustrate the frequency responses of the vertical FG pipe ($\chi = 0$) at two different temperatures in its post-buckled state. It may be observed from these results (Fig. 5b–c) and the results in Fig. 4 that the motion of the FG pipe is primarily associated with its positive or negative post-buckled equilibrium position, where the oscillation of the FG pipe amplifies indicatively via the principal primary and secondary parametric resonances at the frequencies of 2 Ω_n and Ω_n, respectively. Here, the principal primary parametric resonance develops through the period doubling/period demultiplying bifurcation and the stable periodic motion evolves at the points A/A′ or B/B′ (Fig. 5b) through the period demultiplying bifurcation as the corresponding global bifurcation diagram (Fig. 5d) reveals it to occur within a very small frequency band (near A/A′ or B/B′, Fig. 5d). However, at a higher temperature (Fig. 5c), the same stable periodic motion appears through the saddle–node bifurcation (K/K′, L/L′, Fig. 5c). It may also be observed from Fig. 5b–c that the unstable (post-buckled) equilibrium point (saddle–node, OO′) lies over the zero line ($\eta_m = 0$) and the mean point of oscillation (black line) shifts from the stable (post-buckled) equilibrium point towards the zero-line ($\eta_m = 0$) especially when the oscillation of the FG pipe amplifies via the resonances.

Apart from these local oscillatory motions of the FG pipe with respect to the post-buckled equilibrium points, Fig. 5b shows the appearance of a global periodic oscillation (period-2, QR/Q′R′ in Fig. 5b) of the FG pipe encircling the positive and negative buckled equilibrium points. Although this global periodic oscillation disappears at a higher temperature (Fig. 5c), it is basically snap-through periodic motion of the FG pipe. A similar observation in case of the vertical isotropic pipe is also reported in [50].

The FG pipe is now taken at an inclined orientation ($\chi = 25°$), and its frequency responses in the pre-buckled state are shown in Fig. 6a and b for two different temperatures (T_i) as 300 K and 335 K, respectively. Comparing with the responses at the pre-buckled state of the FG pipe in Figs. 5a and 6a, the inclination of the FG pipe causes a shift of its static equilibrium position towards the negative side ($\eta_m < 0$) due to the gravitational load, and also the principal secondary parametric resonance (fundamental resonance) appears along with the principal primary one. Additionally, there is a little shift of the mean point of oscillation (black line, Fig. 6a) from the static equilibrium point specifically when the inclined FG pipe undergoes principal primary parametric resonance. Here, the principal primary parametric resonance appears through the period doubling/period demultiplying bifurcation (Fig. 6a) instead of the pitchfork bifurcation (Fig. 5a) in the case of the vertical FG pipe. However, at a higher temperature (T_i = 335 K, Fig. 6b) in the same (pre-buckled) equilibrium state, the transverse deflection of the inclined FG pipe appears indicatively (Fig. 4), and thus the softening structural behavior of the FG pipe appears in addition to

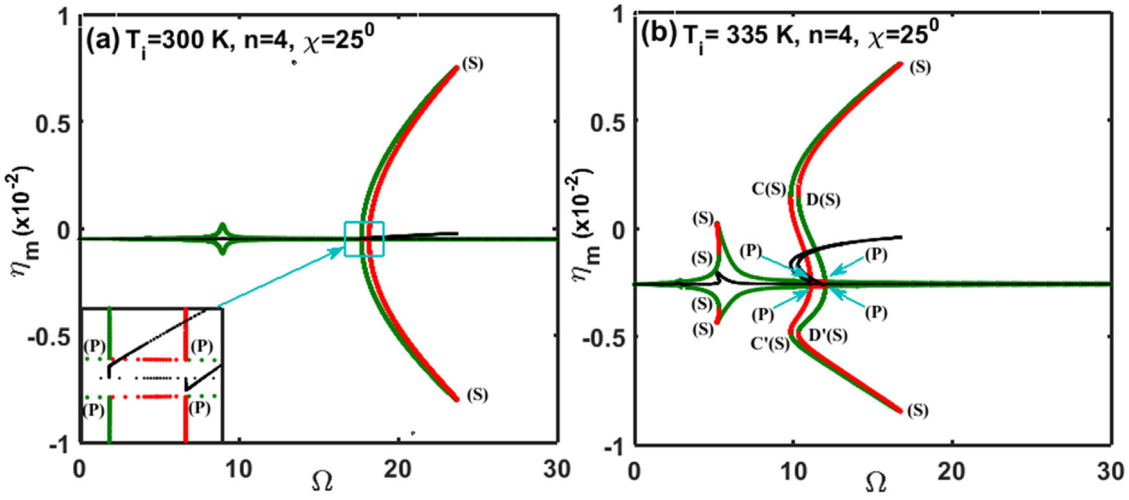

Fig. 6. Nonlinear frequency responses of inclined FG pipe ($n = 4$, $\lambda = 0.5$, $V_f = 5$ m/s, $\chi = 25^0$) in the pre-buckled state with different temperatures; (a) $T_i = 300$ K, (b) $T_i = 335$ K.

the hardening one as shown in Fig. 6b for the response via principal parametric resonance. In fact, the mean point of oscillation (black line, Fig. 6b) shifts towards the zero-line ($\eta_m = 0$), and it results in lesser curvature of the FG pipe at some frequencies leading to the appearance of its (pipe) hardening behavior. The corresponding exchange between the hardening and softening behavior of the FG pipe occurs through the saddle–node bifurcation (C/C', D/D', Fig. 6b). It may also be observed from Fig. 6a–b that the oscillation of the inclined FG pipe via the fundamental resonance amplifies due to the increase of temperature (T_i) and the corresponding bifurcations (Fig. 6b) of the stable periodic oscillation occurs through the saddle–node bifurcation.

As the temperature (T_i) increases, the inclined FG pipe undergoes divergence instability (buckling). The corresponding frequency response of the inclined FG pipe is illustrated in Fig. 7a for an inclination angle (χ) of 15^0. In contrast to the response of the vertical FG pipe (Fig. 5b) in its post-buckled state, the response of the inclined FG pipe in Fig. 7a exhibits unequal amplitudes of oscillation corresponding to its positive and negative buckled equilibrium positions, and it appears due to the asymmetric buckled equilibrium positions of the inclined FG pipe with respect to the zero-line ($\eta_m = 0$). However, the local primary parametric resonance about the buckled equilibriums appears through the period doubling/period demultiplying (Fig. 7a) similar to the response in Fig. 5b. Also, for the response in Fig. 7a, the stable periodic oscillation of the inclined FG pipe corresponding to the local primary parametric resonance arises through the period demultiplying bifurcations at points A/A′ and B/B′ (Fig. 7a) similar to the response in Fig. 5b. Additionally, similar stable periodic oscillation about the negative buckled equilibrium also arises in a very small frequency region through the saddle–node bifurcation (E/E′, Fig. 7a). The saddle–node bifurcation appears at all other points of bifurcation (Fig. 7b) except the point F/F′ where the period demultiplying bifurcation appears. Similar to the response in Fig. 5b for vertical FG pipe, the response (Fig. 7a) of the inclined FG pipe involves both the global and local motions in a certain frequency range. But, the saddle–node (OO′, Fig. 5b) in the response of the vertical FG pipe becomes saddle periodic orbit (over OO', Fig. 7a) due to the inclination. This saddle periodic orbit shifts towards the positive side ($\eta_m > 0$) from the zero-line ($\eta_m = 0$), and it results in smaller domain of attraction over the positive buckled equilibrium point than that over the negative buckled equilibrium point as it is shown in Fig. 7c through the plot of the basin of attraction, as well as the limit cycle attractors (green closed curves) and saddle periodic orbit (red closed curves), at a frequency of $\Omega = 9$.

For an increase of the inclination angle (χ) from 15^0 to 45^0, the corresponding changes of the frequency response can be observed from Fig. 7(a) and (b), where it is clear that the static equilibrium state of the FG pipe changes from post-buckled to pre-buckled state at the same temperature leading to simpler response. For the response in Fig. 7b at a higher inclination angle ($\chi = 45°$) of the FG pipe, the stable periodic motion via principal primary parametric resonance arises through the period doubling/period demultiplying (F/F′ and B/B′) and saddle–node (E/E′) bifurcations, whereas the bifurcation of stable periodic motion via the fundamental resonance occurs through the saddle–node bifurcation (Fig. 7b). However, the responses of the inclined FG pipe in Fig. 7a–b show an indicative effect of the inclination angle on its (FG pipe) nonlinear dynamic characteristics.

Figs. 6a–b and 8a–d illustrate the changes in the nonlinear dynamic characteristics of the inclined FG pipe ($\chi = 25°$) with the gradual increase of temperature (T_i) as 300 K, 335 K, 344 K, 355 K, 385 K and 390 K. As the temperature increases from the room temperature (300 K) to 335 K or 344 K, the thermal deflection of the inclined FG pipe increases resulting in the simultaneous appearance of hardening and softening structural behavior of the pipe (Figs. 6b and 8a). The corresponding exchange between the softening and hardening structural behavior occurs either through the saddle–node bifurcation (C/C′ and D/D′, Figs. 6b and 8a) or through the period doubling/period demultiplying bifurcation (B/B′ and F/F′, Fig. 8a). However, for further increase of temperature ($T_i = 355$ K, Fig. 8b), the inclined FG pipe undergoes buckling leading to the nonlinear frequency response as shown in Fig. 8b. The response in Fig. 8b is almost similar to that in Fig. 7a, however, the only difference is in the appearance of the global motion of the FG pipe. It is observed that this global motion of the FG pipe appears for its low curvature that usually occurs at the post-buckled equilibrium near the onset of buckling (divergence). However, it is important to notice from Fig. 8b or Fig. 7a that the natural frequency and the amplitude of oscillation of the FG pipe do not appear in an equal manner over its two buckled equilibriums, and it arises due to the difference in the corresponding curvatures of the inclined pipe.

For further increase of temperature ($T_i = 385$ K, Fig. 8c), the local principal primary parametric resonance corresponding to the buckled equilibrium on the negative side ($\eta_m < 0$) disappears. However, the same also occurs corresponding to the buckled equilibrium on the positive side ($\eta_m > 0$) for a little more temperature ($T_i = 390$ K, Fig. 8d). This may be due to the fact that the nonlinear stiffness or curvature of the inclined FG pipe increases at a higher temperature (T_i). However, it is important to observe from Fig. 8d and Fig. 5c that the frequency response of the inclined FG pipe is almost similar to that for the vertical FG pipe, and it occurs at a high temperature in the post-buckled state of the FG pipe. It may also be observed from Fig. 8b, c and d that the saddle periodic orbit (OO′, Fig. 8) shifts towards the zero-line ($\eta_m = 0$)

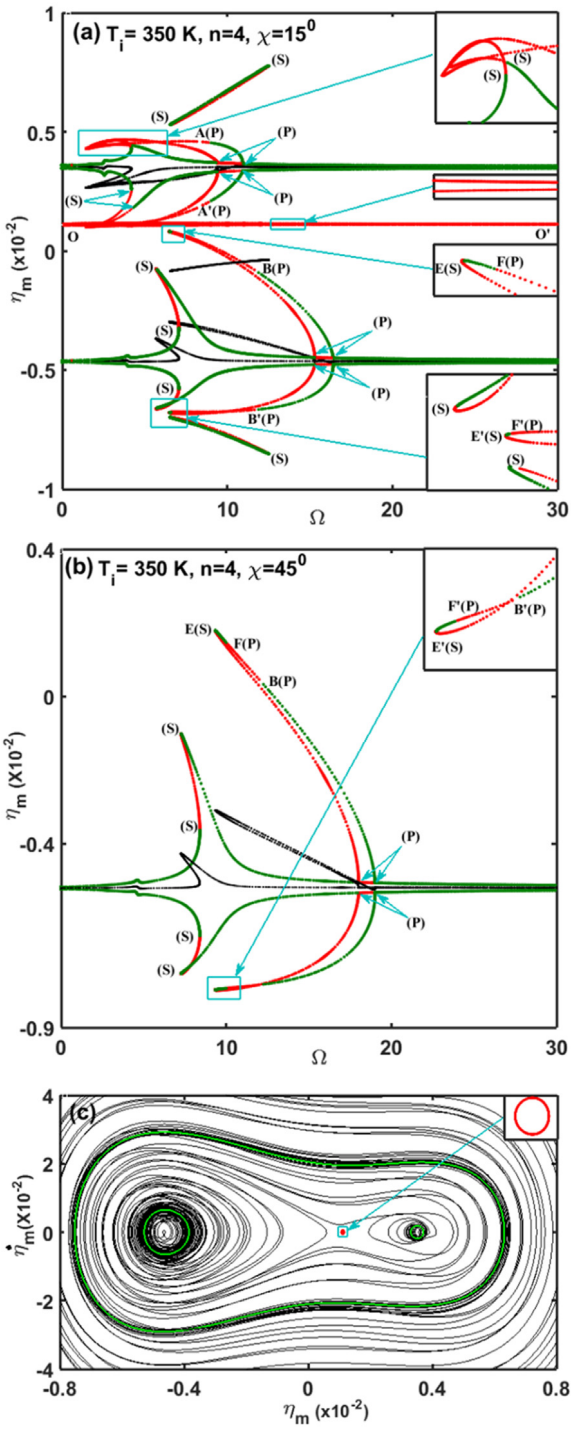

Fig. 7. Nonlinear frequency responses of the inclined FG pipe ($n = 4$, $\lambda = 0.5$, $V_f = 5$ m/s) with (a) $\chi = 15^0$, $T_i = 350$ K, (b) $\chi = 45^0$, $T_i = 350$ K, (c) basin of attraction at a frequency of $\Omega = 9$ corresponding to the response in Fig. 7a. (For interpretation of the references to color in this figure legend, the reader is referred to the web version of this article.)

with the increase of temperature leading to almost equal domains of attraction over the positive and negative post-buckled equilibriums. It is corroborated in Fig. 9 through the plot of the basin of attraction at two different temperatures ($T_i = 355$ K, $T_i = 385$ K) with $\Omega = 7.5$. From these observations, it may be concluded that the nonlinear dynamic characteristics of the inclined FG pipe at a high temperature in its post-buckled state approach to that of the vertical FG pipe so that the angle of inclination of the FG pipe has minimal effect on its dynamic behavior.

5.3.2. Effect of graded exponent

A higher value of the graded exponent (n) of FGM means more volume fraction of the metal constituent resulting in softer FG pipe. Also, the corresponding decrease of the volume fraction of the ceramic constituent yields higher temperature at any point within the wall-thickness of the FG pipe under the specified surface temperatures. These two factors result in higher deflection of the FG pipe for an increase of the graded exponent without any change of the surface temperatures. Now, at a low temperature i.e. at the pre-buckled state of the FG pipe, its static profile or curvature appears because of its inclination ($\chi \neq 0$) (Fig. 4). This static deflection increases for a higher value of the graded exponent due to the aforesaid reasons. The effect of this greater static deflection on the dynamics of the inclined FG pipe ($\chi = 25°$) conveying pulsatile fluid ($V_f = 5$ m/s, $\lambda = 0.5$) is illustrated in Figs. 8a and 10a for an increase in the value of the graded exponent from 4 to 8 at a temperature (T_i) of 344 K. These results indicate the disappearance of the hardening structural behavior of the inclined FG pipe for an increase of the graded exponent. In contrast, similar change would not appear for a vertical FG pipe ($\chi = 0°$), where the vertical FG pipe always behaves as a hardening structure as there is no initial static deflection at its pre-buckled state (at a low temperature) (Fig. 4).

At the post-buckled state of the inclined FG pipe, the aforesaid result indicates that the two (positive and negative) buckled equilibrium positions of the pipe are not symmetric with respect to the zero-line ($\eta_m = 0$), and it appears due to an inclination angle of the pipe. However, for an increase of the graded exponent (n) at a constant surface temperature (T_i), the curvature of the FG pipe corresponding to its positive/negative post-buckled equilibrium states increases. The corresponding effects on the dynamics of the inclined FG pipe ($\chi = 25°$) at its post-buckled state are illustrated in Figs. 10b and 8b for an increase of the graded exponent from 2 to 4. It may be observed from these figures (Figs. 10b and 8b) that the global parametric resonance may disappear due to the increased curvature of the FG pipe at a higher value of the graded exponent. Also, for the increase of the graded exponent, the buckled equilibrium positions tends to be symmetric with respect to the zero-line ($\eta_m = 0$) leading to the similar dynamic responses of the inclined FG pipe over its positive and negative post-buckled equilibrium positions. So, a higher value of the graded exponent (n) of FGM yields reduced effect of the inclination angle on the dynamic characteristics of the FG pipe in its post-buckled state.

5.3.3. Effect of flow velocity and pulsation amplitude

The motion of the inclined pinned–pinned FG pipe arises due to the pulsatile flow of internal fluid where the excitation parameters are the mean flow velocity (V_f) and the pulsation amplitude (λ). So, the effects of these parameters on the dynamics of the inclined FG pipe are investigated in this section. Figs. 8a and 11a illustrate the nonlinear frequency responses of the inclined FG pipe ($\chi = 25°$) at its pre-buckled state for two different values of the mean flow velocity (V_f) as 5 m/s and 3m/s, respectively. It may be observed from these results (Figs. 8a and 11a) that the curvature of the inclined FG pipe at its pre-buckled state increases for a higher mean flow velocity since the corresponding compressive stress in the pipe increases. Additionally, a higher mean flow velocity causes the oscillation of the inclined FG pipe with a greater displacement amplitude, where also a greater shift of the mean point of oscillation (black line) towards the zero-line ($\eta_m = 0$) appears resulting in the appearance of the hardening structural behavior of the inclined FG pipe. In contrast, the vertical FG pipe has no initial curvature at its pre-buckled state, and thus it always behaves as a hardening structure. However, the amplitude of oscillation of the vertical FG pipe is expected to vary with the change of the mean flow velocity.

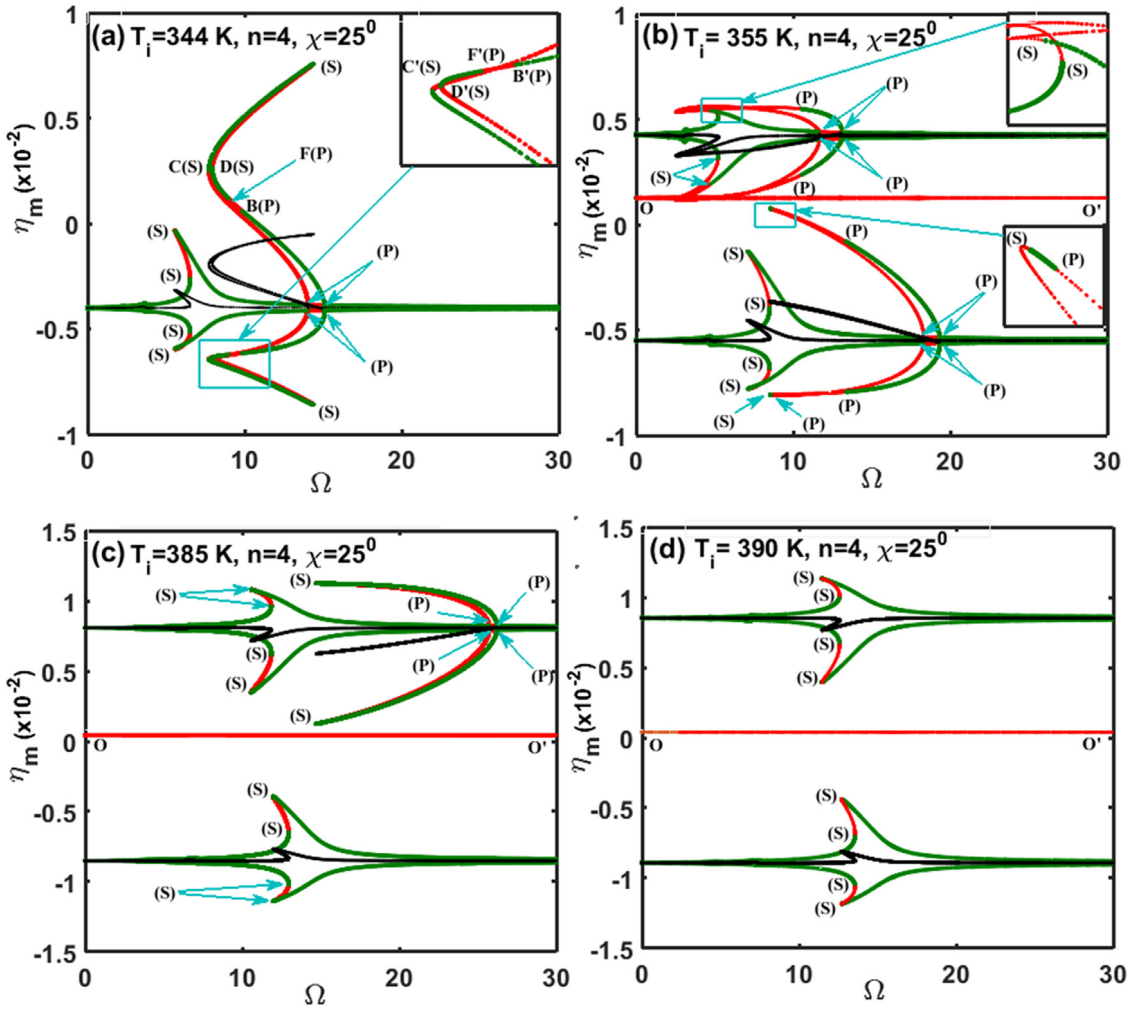

Fig. 8. Nonlinear frequency responses of the inclined FG pipe ($n = 4$, $\lambda = 0.5$, $V_f = 5$ m/s, $\chi = 25^0$) for different temperatures; (a) $T_i = 344$ K, (b) $T_i = 355$ K, (c) $T_i = 385$ K and (d) $T_i = 390$ K.

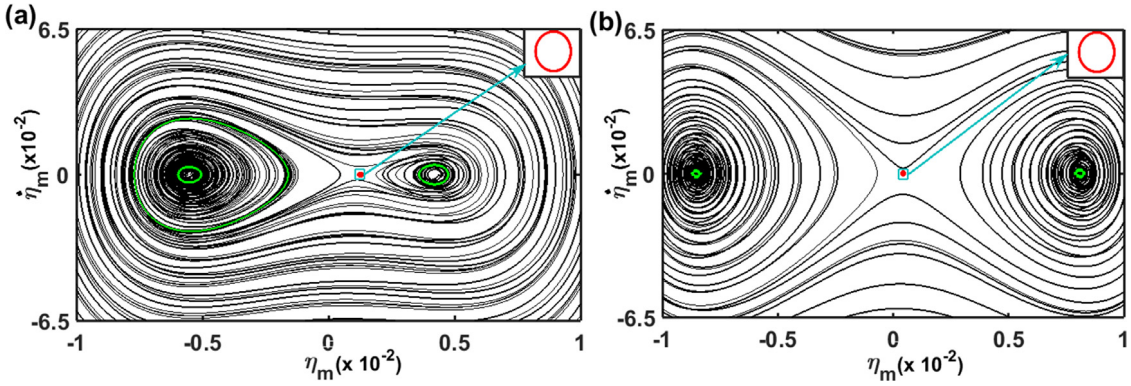

Fig. 9. Basin of attraction at a frequency of $\Omega = 7.5$ ($n = 4$, $\lambda = 0.5$, $V_f = 5$ m/s, $\chi = 25^0$) for two different temperatures; (a) $T_i = 355$ K and (b) $T_i = 385$ K (green closed curves are limit cycle attractors and red closed curve is saddle periodic orbit). (For interpretation of the references to color in this figure legend, the reader is referred to the web version of this article.)

In the case of a decrease of the mean flow velocity in the post-buckled state of the inclined FG pipe, Figs. 8b and 11b illustrate the corresponding changes in its (FG pipe) nonlinear dynamic behavior. It is clear from these results (Figs. 8b and 11b) that the principal primary parametric resonance over the negative ($\eta_m < 0$) post-buckled equilibrium position disappears for a decrease of the mean flow velocity. Also, the displacement amplitude of oscillation of the inclined FG pipe decreases. These observations infer simpler dynamics of the inclined FG pipe in its post-buckled state for a low mean flow velocity. Similar changes in the nonlinear dynamic characteristics of the pre or post-buckled inclined FG pipe are also observed for the variation of the pulsation amplitude (λ), and thus these results are not furnished here.

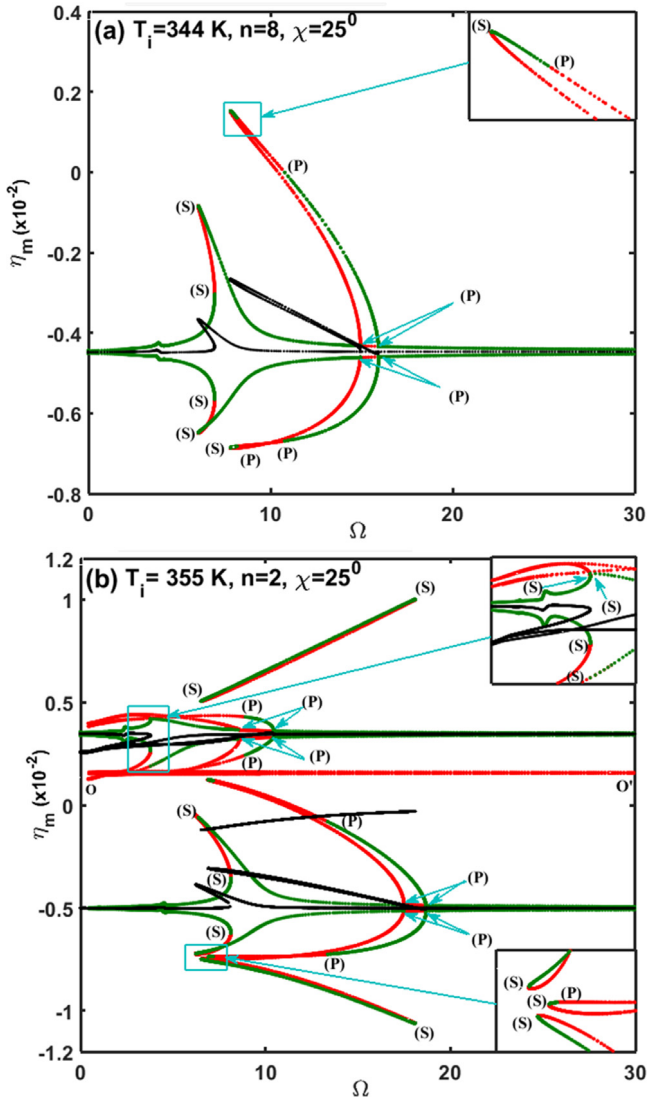

Fig. 10. Nonlinear frequency responses of the inclined FG pipe (V_f = 5 m/s, λ = 0.5, χ = 25^0) for (a) T_i = 344 K, n = 8, (b) T_i = 355 K, n = 2.

5.3.4. *Effect of material damping of FGM*

The material damping of the FGM is presently considered through its metal constituent with the assumption of no material damping in the ceramic constituent. The corresponding coefficient of Kelvin–Voigt dissipation parameter or retardation time (r_τ) for the metal constituent is considered as 0.0004 s [45] in the evaluation of the aforesaid nonlinear dynamic responses of the FG pipe. However, for investigating the effect of the material damping of FGM on the dynamic behavior of the inclined FG pipe, the same parameter (r_τ) is taken with a lower value as 0.00004 s, and the earlier results in Figs. 7b and 8d are reevaluated as presented in Figs. 12a and 13a corresponding to the pre-buckled and post-buckled states of the inclined FG pipe, respectively.

For the pre-buckled state, it can be observed from Figs. 7b and 12a that the oscillation of the inclined FG pipe is amplified indicatively due to its (FG pipe) reduced material damping. Also, the oscillation of the FG pipe via parametric resonances appears in a wide range of frequency. More importantly, the hardening structural behavior of the FG pipe appears along with its softening behavior for both the principal primary and secondary parametric resonances (Fig. 12a). However, the frequency responses in Figs. 7b and 12a indicate a little more complex dynamic behavior of the inclined FG pipe in its pre-buckled state for a decrease of material damping of FGM. For a clarification of the corresponding bifurcation of motion of the inclined FG pipe, the global bifurcation diagram is illustrated in Fig. 12b for the frequency response in Fig. 12a. It may be observed from Fig. 12b that the bifurcation of periodic oscillation via principal primary parametric resonance occurs through period doubling/period demultiplying bifurcation while the bifurcation of similar motion via fundamental resonance occurs through saddle–node bifurcation similar to that for the response in Fig. 8a. However, the higher order parametric resonance is also observed (Fig. 12a) for the low material damping. In the frequency region between U/U' and V/V', a period-4 attractor is also observed (Fig. 12b) along with the period-1 attractor via the fundamental resonance. These observations indicate the material damping of FGM as an important factor not only to attenuate the oscillation but also to reduce the complex nonlinear dynamic behavior of the FG pipe.

In the post-buckled state of the inclined FG pipe, the changes in its nonlinear dynamics for the aforesaid decrease of the material damping of FGM are clarified though the results in Figs. 8d and 13a. As displayed in these results (Figs. 8d and 13a), the nonlinear dynamic response of the inclined FG pipe appears in a complex manner for a decrease of the material damping of FGM. This complex dynamic behavior of the inclined FG pipe arises mainly due to the extended response of the FG pipe over a wide range of frequency and also due to the appearance of the higher order parametric resonance (zoomed part in Fig. 13a). However, the corresponding global bifurcation diagram (Fig. 13b) reveals similar kinds of bifurcations of the periodic motion of the inclined FG pipe as that are observed for the response in Fig. 5b.

6. Conclusions

In this work, the nonlinear dynamics of a pinned–pinned inclined FG pipe conveying hot fluid with pulsatile flow velocity is studied. The FG pipe is comprised of metal and ceramic constituents with the inner ceramic rich surface to withstand the high temperature of internal hot fluid. The slender FG pipe is modeled using Euler–Bernoulli beam theory while the fluid flow is modeled by the assumption of plug-flow. The governing equation of motion is derived employing Hamilton's principle, and subsequently it is solved through the Galerkin discretization, where the IHB method and adaptive Runge–Kutta method are employed for evaluation of the numerical results in the frequency and time domains, respectively.

First, the effects of the gravitational load and the temperature of the internal fluid on the static deflection of the inclined FG pipe are investigated for its (pipe) different inclination angles with the vertical axis, where the internal mass of fluid is considered with or without steady flow velocity. This investigation reveals the following static deformation and instability characteristics of the inclined FG pipe.

(a) The initial static deflection of the FG pipe due to the gravitational force does not alter indicatively for the steady flow velocity of the internal fluid. However, the static deflection of the FG pipe increases indicatively for an increase of the temperature of the internal fluid and also for an increase in the value of the graded exponent of FGM.
(b) If the vertical orientation of an FG pipe changes to inclined one, then the buckling of the pipe occurs through the saddle–node bifurcation instead of the pitchfork bifurcation.
(c) The critical buckling temperature of the inclined FG pipe increases as the inclination angle and/or the graded exponent of FGM increase.

Next, the dynamics of the inclined FG pipe conveying hot fluid with pulsatile flow velocity is studied, where the effects of inclination angle, temperature of the internal fluid and graded exponent of FGM on the dynamic characteristics of the inclined FG pipe are mainly investigated corresponding to its pre-buckled and post-buckled equilibrium states. The present results for the dynamics of the inclined FG pipe at its pre-buckled state reveal the following main observations.

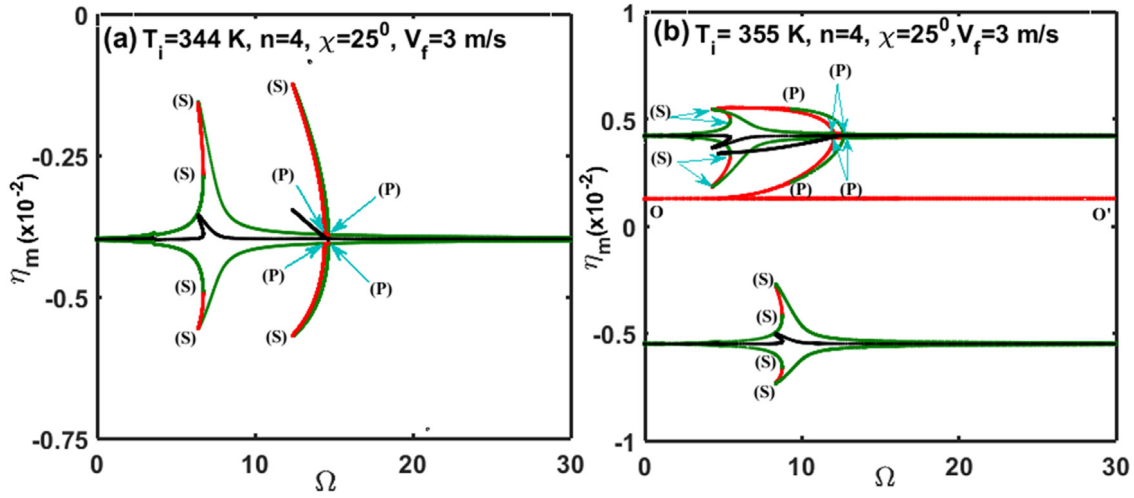

Fig. 11. Nonlinear frequency responses of the inclined FG pipe ($n = 4$, $\lambda = 0.5$, $\chi = 25^0$) conveying pulsatile fluid with the flow velocity (V_f) of 3 m/s at two different temperatures; (a) $T_i = 344$ K and (b) $T_i = 355$ K.

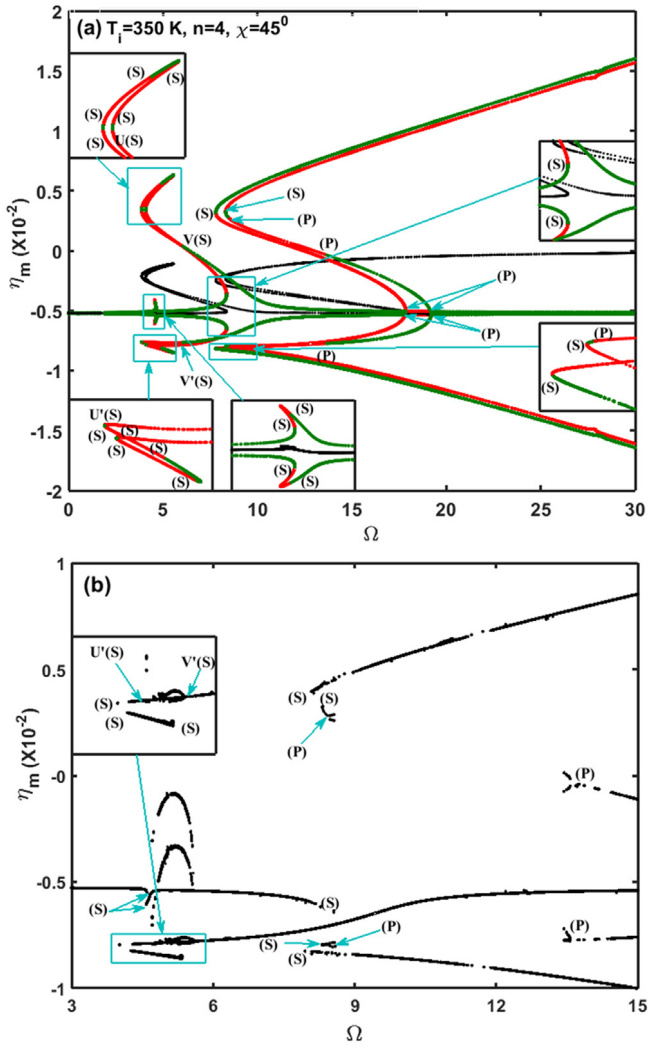

Fig. 12. (a) Nonlinear frequency response of the inclined FG pipe at its pre-buckled state ($T_i = 350$ K, $\chi = 45^0$) for a low material damping of FGM ($r_z = 0.00004$ s, $V_f = 5$ m/s, $\lambda = 0.5$) and (b) the corresponding global bifurcation diagram.

(a) The FG pipe undergoes principal primary parametric resonance in its pre-buckled state. However, the inclination of the FG pipe from its vertical orientation causes the appearance of this resonance through the period doubling/period demultiplying bifurcation instead of the pitchfork bifurcation.

(b) An inclined FG pipe undergoes both the principal primary and secondary parametric resonances in its pre-buckled state. The corresponding amplitude of vibration of the FG pipe increases indicatively for an increase of the temperature of internal fluid and also for a high value the graded exponent of FGM.

(c) For the oscillation of the inclined FG pipe under the principal primary parametric resonance, the deflection of the FG pipe at the mean point of oscillation may arise with a low value. It results in the appearance of the hardening structural behavior of the inclined FG pipe at a certain range of frequency of vibration, and the FG pipe exhibits either softening or hardening structural behavior during its vibration at a frequency within the same frequency range. The corresponding exchange of structural behavior of the inclined FG pipe occurs through the saddle–node/period doubling/period demultiplying bifurcation.

(d) The hardening structural behavior of the inclined FG pipe may disappear for an increase of one of the system parameters like temperature of the internal fluid, graded exponent of FGM and inclination angle. However, despite the high values of these system parameters, the hardening structural behavior of the inclined FG pipe may retain for high mean flow velocity and/or high velocity–amplitude of pulsating fluid flow.

As the temperature of the internal fluid increases, the post-buckled state of the inclined FG pipe arises with two possible static equilibrium states that are identified as the negative and positive post-buckled equilibrium states following the corresponding deflections of the FG pipe along and opposite to its initial deflection under the gravitational load. However, the present investigation on the dynamics of the inclined FG pipe at its post-buckled state reveals the following salient observations.

(a) A stable global periodic oscillation of the inclined FG pipe encircling the positive and negative post-buckled equilibrium states may appear when the post-buckled state of the pipe is near the onset of buckling. This global periodic attractor appears along with the other two local periodic attractors corresponding to the positive and negative post-buckled equilibrium states.

(b) If the temperature of the internal fluid increases gradually from the critical buckling temperature, then the principal primary parametric resonance disappears in the dynamic response the

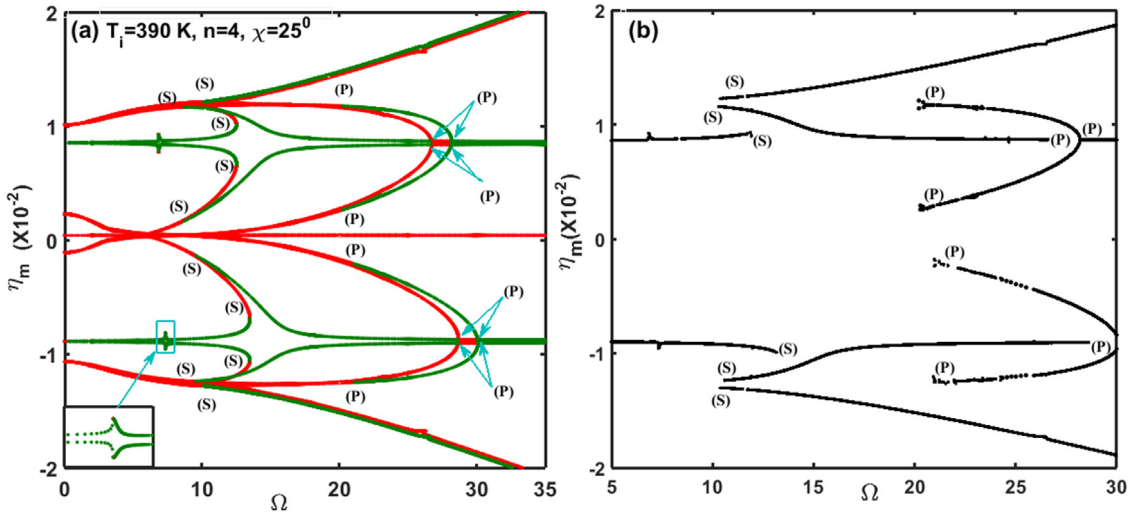

Fig. 13. (a) Nonlinear frequency response of the inclined FG pipe at its post-buckled state ($T_i = 390$ K, $\chi = 25^0$) for a low material damping of FGM ($r_\tau = 0.00004$ s, $V_f = 5$ m/s, $\lambda = 0.5$) and (b) the corresponding global bifurcation diagram.

FG pipe with respect to the negative post-buckled equilibrium state. The same also occurs in the dynamic response of the FG pipe with respect to the positive post-buckled equilibrium state for further increase of the temperature.

(c) In the dynamic response of the inclined FG pipe at its post-buckled state, the saddle periodic orbit arises instead of the saddle–node. This saddle periodic orbit shifts towards the positive post-buckled equilibrium state due to an increase of the inclination angle or a decrease of the temperature, and it results in unequal domains of attraction over the positive and negative post-buckled equilibrium states.

(d) For the low material damping of FGM, the inclined FG pipe undergoes higher order parametric resonances along with the principal parametric resonances.

(e) At very high temperature of the internal fluid, the dynamic responses of the inclined FG pipe at its post-buckled state become similar to that of the vertical FG pipe.

Declaration of competing interest

The authors declare that they have no known competing financial interests or personal relationships that could have appeared to influence the work reported in this paper.

Funding

This research did not receive any specific grant from funding agencies in the public, commercial, or not-for-profit sectors.

References

[1] M.P. Paidoussis, Fluid–Structure Interactions: Slender Structures and Axial Flow, Vol. 1, Academic press, London, 2014.
[2] R.A. Ibrahim, Overview of mechanics of pipes conveying fluids—Part I: Fundamental studies, J. Press. Vessel Technol. 132 (2010) 034001–1–034001–32.
[3] M.P. Paidoussis, N.T. Issid, Experiments on parametric resonance of pipes containing pulsatile flow, J. Appl. Mech. 43 (1976) 198–202.
[4] M.P. Paidoussis, G.X. Li, Pipes conveying fluid: a model dynamical problem, J. Fluids Struct. 7 (1993) 137–204.
[5] E. Tubaldi, M. Amabili, M.P. Païdoussis, Fluid–structure interaction for nonlinear response of shells conveying pulsatile flow, J. Sound Vib. 371 (2016) 252–276.
[6] M. Amabili, F. Pellicano, M.P. Païdoussis, Non-linear dynamics and stability of circular cylindrical shells containing flowing fluid. Part I: stability, J. Sound Vib. 225 (1999) 655–699.
[7] P.J. Holmes, Pipes supported at both ends cannot flutter, J. Appl. Mech. 45 (1978) 619–622.
[8] A.K. Bajaj, P.R. Sethna, T.S. Lundgren, Hopf bifurcation phenomena in tubes carrying a fluid, SIAM J. Appl. Math. 39 (1980) 213–230.
[9] J. Rousselet, G. Herrmann, Dynamic behavior of continuous cantilevered pipes conveying fluid near critical velocities, J. Appl. Mech. 48 (1981) 943–947.
[10] S. Chen, Dynamic stability of tube conveying fluid, J. Eng. Mech. 97 (1971) 1469–1485.
[11] M.P. Paidoussis, N.T. Issid, Dynamic stability of pipes conveying fluid, J. Sound Vib. 33 (1974) 267–294.
[12] M.P. Paidoussis, C. Sundararajan, Parametric and combination resonances of a pipe conveying pulsating fluid, J. Appl. Mech. 42 (1975) 780–784.
[13] S.T. Ariaratnam, N.S. Namachchivaya, Dynamic stability of pipes conveying pulsating fluid, J. Sound Vib. 107 (1986) 215–230.
[14] N. Sri Namchchivaya, W.M. Tien, Non-linear dynamics of supported pipe conveying pulsating fluid-II. Combination resonance, Int. J. Nonlinear Mech. 24 (1989) 197–208.
[15] J.D. Jin, Z.Y. Song, Parametric resonances of supported pipes conveying pulsating fluid, J. Fluids Struct. 20 (2005) 763–783.
[16] A. Czerwiński, J. Łuczko, Parametric vibrations of flexible hoses excited by a pulsating fluid flow, Part II: Experimental research, J. Fluids Struct. 55 (2015) 174–190.
[17] E. Tubaldi, M. Amabili, M.P. Païdoussis, Nonlinear dynamics of shells conveying pulsatile flow with pulse-wave propagation. Theory and numerical results for a single harmonic pulsation, J. Sound Vib. 396 (2017) 217–245.
[18] Y. dong Li, Y. ren Yang, Nonlinear vibration of slightly curved pipe with conveying pulsating fluid, Nonlinear Dynam. 88 (2017) 2513–2529.
[19] L. Wang, H.L. Dai, Q. Qian, Dynamics of simply supported fluid-conveying pipes with geometric imperfections, J. Fluids Struct. 29 (2012) 97–106.
[20] J. Łuczko, A. Czerwiński, Parametric vibrations of flexible hoses excited by a pulsating fluid flow, Part I: Modelling, solution method and simulation, J. Fluids Struct. 55 (2015) 155–173.
[21] Y.-L. Zhang, L.-Q. Chen, Steady-state response of pipes conveying pulsating fluid near a 2:1 internal resonance in the supercritical regime, Int. J. Appl. Mech. 06 (2014) 1450056.
[22] H.L. Dai, L. Wang, Q. Qian, Q. Ni, Vortex-induced vibrations of pipes conveying fluid in the subcritical and supercritical regimes, J. Fluids Struct. 39 (2013) 322–334.
[23] B. Gültekin Sinir, Pseudo-nonlinear dynamic analysis of buckled pipes, J. Fluids Struct. 37 (2013) 151–170.
[24] J. Deng, Y. Liu, Z. Zhang, W. Liu, Stability analysis of multi-span viscoelastic functionally graded material pipes conveying fluid using a hybrid method, Eur. J. Mech. A Solids 65 (2017) 257–270.
[25] Y.L. Zhang, L.Q. Chen, External and internal resonances of the pipe conveying fluid in the supercritical regime, J. Sound Vib. 332 (2013) 2318–2337.
[26] Q. Qian, L. Wang, Q. Ni, Instability of simply supported pipes conveying fluid under thermal loads, Mech. Res. Commun. 36 (2009) 413–417.
[27] M. Koizumi, The concept of FGM, Ceram. Trans. Funct. Gradient Mater. 34 (1993) 3–10.
[28] M. Hosseini, S.A. Fazelzadeh, Thermomechanical stability analysis of functionally graded thin-walled cantilever pipe with flowing fluid subjected to axial load, Int. J. Struct. Stab. Dyn. 11 (2011) 513–534.

[29] M. Eftekhari, M. Hosseini, On the stability of spinning functionally graded cantilevered pipes subjected to fluid-thermomechanical loading, Int. J. Struct. Stab. Dyn. 16 (2016) 1550062.
[30] S. Lips, J.P. Meyer, Two-phase flow in inclined tubes with specific reference to condensation: A review, Int. J. Multiph. Flow 37 (2011) 845–859.
[31] X. Wang, F. Bloom, Stability issues of concentric pipes containing steady and pulsatile flows, J. Fluids Struct. 15 (2001) 1137–1152.
[32] U. Lee, J. Kim, Dynamics of branched pipeline systems conveying internal unsteady flow, J. Vib. Acoust. 121 (1999) 114–122.
[33] P. Vigneaux, P. Chenais, J.P. Hulin, Liquid-liquid flows in an inclined pipe, AIChE J. 34 (1988) 781–789.
[34] R. Dawson, P.R. Paslay, Drillpipe buckling in inclined holes, J. Pet. Technol. (1984) 1734–1738.
[35] F.K. Alfosail, A.H. Nayfeh, M.I. Younis, Natural frequencies and mode shapes of statically deformed inclined risers, Int. J. Nonlinear Mech. 94 (2017) 12–19.
[36] X. Wang, F. Bloom, Dynamics of a submerged and inclined concentric pipe system with internal and external flows, J. Fluids Struct. 13 (1999) 443–460.
[37] C. Gan, S. Jing, S. Yang, H. Lei, Effects of supported angle on stability and dynamical bifurcations of cantilevered pipe conveying fluid, Appl. Math. Mech. 36 (2015) 729–746, English Ed.
[38] W.N. Findley, F.A. Davis, Creep and Relaxation of Nonlinear Viscoelastic Materials, Courier Corporation, 2013.
[39] P.A. Kadam, S. Panda, Nonlinear analysis of an imperfect radially graded annular plate with a heated edge, Int. J. Mech. Mater. Des. 10 (2014) 281–304.
[40] P.J. Holmes, Bifurcations to divergence and flutter in flow-induced oscillations: A finite dimensional analysis, J. Sound Vib. 53 (1977) 471–503.
[41] J.J. Thomsen, Vibrations and Stability: Advanced Theory, Analysis, and Tools, Springer Science & Business Media, 2013.
[42] P. Friedman, C.E. Hammond, T.H. Woo, Efficient numerical treatment of periodic systems with application to stability problems, Internat. J. Numer. Methods Engrg. 11 (1977) 1117–1136.
[43] T. Fuchiyama, N. Noda, Analysis of thermal stress in a plate of functionally gradient material, JSAE Rev. 16 (1995) 263–268.
[44] H.-S. Shen, Functionally Graded Materials: Nonlinear Analysis of Plates and Shells, CRC press, 2016.
[45] A. Bommakanti, S. Roy, S. Suwas, Effect of hypoeutectic boron modification on the dynamic properties of Ti-6Al-4V alloy, J. Mater. Res. 31 (2016) 2804–2816.
[46] A. Kumar, S. Panda, S. Kumar, D. Chakraborty, A design of laminated composite plates using graded orthotropic fiber-reinforced composite plies, Compos. Part B Eng. 79 (2015) 476–493.
[47] Y. Fu, J. Zhong, X. Shao, Y. Chen, Thermal postbuckling analysis of functionally graded tubes based on a refined beam model, Int. J. Mech. Sci. 96–97 (2015) 58–64.
[48] F.K. Alfosail, A.H. Nayfeh, M.I. Younis, An analytic solution of the static problem of inclined risers conveying fluid, Meccanica 52 (2017) 1175–1187.
[49] T. Monprapussorn, C. Athisakul, S. Chucheepsakul, Nonlinear vibrations of an extensible flexible marine riser carrying a pulsatile flow, J. Appl. Mech. 74 (2007) 754–769.
[50] K. Jayaraman, S. Narayanan, Chaotic oscillations in pipes conveying pulsating fluid, Nonlinear Dynam. 10 (1996) 333–357.